AD_____
(Leave blank)

Award Number:
W81XWH-08-1-0701

TITLE:
Micro and Nano-mediated 3D Cardiac Tissue Engineering

PRINCIPAL INVESTIGATOR:
Rashid Bashir, *PhD*

CONTRACTING ORGANIZATION:
University of Illinois
Urbana, IL 61801

REPORT DATE:
October 2010

TYPE OF REPORT:
Annual

PREPARED FOR: U.S. Army Medical Research and Materiel Command
Fort Detrick, Maryland 21702-5012

REPORT DOCUMENTATION PAGE

Form Approved
OMB No. 0704-0188

1. REPORT DATE *(DD-MM-YYYY)*	**2. REPORT TYPE**	**3. DATES COVERED** *(From - To)*
23-OCT-2010	Annual	24 Sep 2009 - 23 Sep 2010

4. TITLE AND SUBTITLE
Micro and Nano-mediated 3D Cardiac Tissue Engineering

5a. CONTRACT NUMBER

5b. GRANT NUMBER
Army W81XWH-08-1-0701

5c. PROGRAM ELEMENT NUMBER

6. AUTHOR(S)
- **Rashid Bashir, *PhD*, PI**

Email: rbashir@uillinois.edu

5d. PROJECT NUMBER

5e. TASK NUMBER

5f. WORK UNIT NUMBER

7. PERFORMING ORGANIZATION NAME(S) AND ADDRESS(ES)
University of Illinois
Urbana, IL 61801

8. PERFORMING ORGANIZATION REPORT NUMBER

9. SPONSORING / MONITORING AGENCY NAME(S) AND ADDRESS(ES)
U.S. Army Medical Research and Materiel
Fort Detrick, Maryland 21702-5012

10. SPONSOR/MONITOR'S ACRONYM(S)

11. SPONSOR/MONITOR'S REPORT NUMBER(S)

12. DISTRIBUTION / AVAILABILITY STATEMENT
Approved for public release; distribution unlimited

13. SUPPLEMENTARY NOTES

14. ABSTRACT: The project envisages improving the care of battlefield-related cardiac injuries by providing novel methods to design and fabricate 3-D models of cardiac sub-components that would be critical in restoring the function of the heart. A commercially-available SLA was modified to accommodate two fabrication methods. We showed significant differences between myocytes extracted from atrium, ventricle and apex *in vitro*-culture. The results suggested that distinguishing the source of myocytes can be crucial for bioengineering myocardium and cell transplantation therapies. In addition, we successfully mobilized stem cells to the peripheral blood in less than 6 hours in the pig model using AMD-3100 (Plerixafor) injections. This new delivery method enables the slow release of an unstable protein-based therapeutic drug over a period of several days. In addition, we have developed a small animal model of myocardial infarction in order to test materials and methods for myocardial repair prior to deployment in a large animal model. A microvascular stamp was developed using microchannels with controlled diameter and spacing into a fibroblast-encapsulated hydrogel using a 3-D stereolithographic fabrication technique. The stamp created is likely to become a powerful tool to better understand vascular biology and improve clinical neovascularization. We also have demonstrated label-free imaging of cell attachment for a variety of cell types including panc-1, HepG2/C3 and cardiomyocytes. The instrument has the ability to monitor changes in cell adhesion over a 24-hour period at the level of individual cells.

15. SUBJECT TERMS
Biomaterials, Biosensors, Fabrication, Mechanobiology

16. SECURITY CLASSIFICATION OF:			**17. LIMITATION OF ABSTRACT**	**18. NUMBER OF PAGES**	**19a. NAME OF RESPONSIBLE PERSON**
U					USAMRMC
a. REPORT	**b. ABSTRACT**	**c. THIS PAGE**	UU	58	**19b. TELEPHONE NUMBER** *(include area code)*
U	U	U			

Standard Form 298 (Rev. 8-98)
Prescribed by ANSI Std. Z39.18

Table of Contents

Contents

Annual Report (Rashid Bashir)

1. Award No. Army W81XWH-08-1-0701
2. Report Date: Oct. 23, 2010
3. Reporting period: 2009-10
4. Principal Investigator: Rashid Bashir, University of Illinois
5. Telephone No.: 217-333-3097
6. Award Organization: University of Illinois
7. Project Title: **Micro and Nano-mediated 3D Cardiac Tissue Engineering**
8. Current staff, role and percent effort of each on project.

Staff Member	**Role**	**% Effort**
Rashid Bashir	PI	2%
Brian Cunningham	Co-PI	2%
Hyunjoon Kong	Co-PI	2%
Taher Saif	Co-PI	2%
Larry Schook	Co-PI	2%
Pinar Zorlutuna	Postdoc Assoc.	100%
Jae Hyun Jeong	Postdoc Assoc.	100%
Emerson De Souza	Postdoc Assoc.	100%
P. Bajaj	Graduate Res. Assistant	50%
V. Chan	Graduate Res. Assistant	50%
Kyle Textor	Graduate Res. Assistant	50%
Vikram Chaudhery	Graduate Res. Assistant	50%
Chun Ge	Graduate Res. Assistant	50%

Award Expenditures: September 24, 2008 to August 31, 2010

Award No. Army W81XWH-08-1-0701

COST ELEMENTS	YEAR 1
Personnel	$394,072
Fringe Benefits	$65,766
Supplies	$106,061
Equipment	$532,852
Travel	$14,724
Other Direct Costs	$49,998
Subtotal	**$1,163,474**
Indirect Costs	$464,953
Fee	$0
Total	**$1,628,427**

Research Groups

I. Rashid Bashir, PI
II. Taher Saif, co-PI
III. Larry Schook, co-PI
IV. Hyun Joon Kong, co-PI
V. Brian Cunningham, co-PI

SECTION I: Annual Report Overall Project

This section describes briefly the salient aspects of the research for the 2009-10 period. Additional details about sub-tasks are provided in subsequent sections.

I. Summary of Work

As an overview, a commercially-available SLA was modified to accommodate for two fabrication methods: (1) the 'top-down' approach, which employed a process similar to the conventional SLA, and (2) the 'bottoms-up' approach, which allowed for multiple cell types and material compositions to be arranged in their own layers within a structure. Laser polymerization characteristics of PEGDA hydrogels were examined and optimized for their utilization in the SLA. We have shown significant differences between myocytes extracted from atrium, ventricle and apex in vitro-culture. The rate of 12 bpm observed for the ventricle is similar to rate of the atrium while the amplitude of 1 μm displacement of ventricle is similar to the apex. With progressing time synchronizations occurs and the amplitudes of ventricle and apex increases by a factor of 5 while the amplitude of atrium myocytes does not change. These results suggest that distinguishing the source of myocytes can be crucial for bioengineering myocardium and cell transplantation therapies.

We have created a microvascular stamp by incorporating microchannels with controlled diameter and spacing into a fibroblast-encapsulated hydrogel using a 3-D stereolithographic fabrication technique. Using this stamp, we demonstrated that we can orchestrate the hydrogel proangiogenic factors along the circular cross-section of the microchannel and form the neovascular pattern equivalent to the pattern engraved into the stamp. The result of our study will be an invaluable paradigm of a 3D cell encapsulation device prepared with a broad array of gel-forming polymers. Specifically, the stamp created in this study will become a powerful tool to better understand vascular biology and also improve quality of a variety of clinical treatments necessitating the neovascularization.

We also have successfully mobilized stem cells to the peripheral blood in less than 6 hours in the pig model using AMD-3100 (Plerixafor) injections. This new delivery method enables the slow release of an unstable protein-based therapeutic drug over a period of several days. In addition, we have developed a small animal model of myocardial infarction in order to test materials and methods for myocardial repair prior to deployment in a large animal model. We also have prepared a rigid and permeable hydrogel with poly(ethylene glycol) diacrylate (PEGDA) and methacrylic alginate (MA), so that the cell-encapsulated hydrogel would not only remain stable at the implanted site but also support cellular expression of proangiogenic factors.

We also have demonstrated label-free imaging of cell attachment for a variety of cell types including panc-1, HepG2/C3 and cardiomyocytes. The instrument has the ability to monitor changes in cell adhesion over a 24-hour period at the level of individual cells, and to monitor the distinct behavior of individual cells within a population. Furthermore, we have established that biosensor can detect differences in the strength of attachment within individual cells and across different cells and to measure changes induced by exposure to drugs. We are continuing to

pursue similar studies to optimize cardiomyocyte cell culture by changing ECM components. Through the use of label-free microscopy using photonic crystal biosensors, we will gain helpful information for defining more effective cardiomyocyte culture protocols in the future.

II. INTRODUCTION

The regeneration of cells and tissue after injury or trauma is critical to medical and civilian communities. Cardiac injuries and regenerative engineering poses specific challenges since cardiac myocytes, the primary cells responsible for the mechanical beating of the heart muscle, do not regenerate. The cardiac system poses a significantly challenging problem in tissue engineering due to the complex 3-dimensional mechano-actuation properties of the cardiac cells. A grand challenge in cardiology since early 50s is the development of an artificial heart that can replace a failing heart. Until today, artificial heart is used only for the temporary use (hrs) until a healthy donor heart is found. The latter is difficult to get, and is often rejected by the body after successful replacement. This very limited success in heart replacement, in spite of considerable effort and resources invested so far, calls for a new paradigm in the approach of heart replacement. This project attempts to offer such a paradigm by proposing to "grow" the heart or its components from the basic building blocks, namely the cells (differentiated cardiomyocytes) of the patient, biomaterials design, namely the hydrogel scaffolds to house the cells, and nanotechnology, namely the stereo-lithographically-patterned 3D substrate. New knowledge on cells' response to mechanical cues, and recent findings on cardiomyocyte functionality on mechanically tuned substrates from our labs form the basis for the project. In summary, stem cell differentiation in scaffolds, novel 3-D fabrication technologies, use of the appropriate biomaterials, integration of peptides for cardiac cell attachment and cell growth, the characterization of the scaffold materials and the transmembrane proteins, and cardiac cell mechanics are all critical elements of a comprehensive design approach proposed in this project for 3-D cardiac tissue engineering.

This project offers a paradigm by proposing to "grow" the heart or its components from the basic building blocks, the cells (differentiated cardiomyocytes) of the patient, biomaterials design of the hydrogels scaffolds to house the cells, use of 3-D stereolithography for fabricating the hydrogel scaffolds with cardiac cells, and nanoscale mechanical and optical tools for characterization of cardiac cells and their interactions with the scaffolds. Our objectives are to integrate these multi-disciplinary efforts and develop the strategies and methodologies for novel designs of 3-D components of an artificial heart.

The project overview and research thrusts for each of the co-PIs are provided in the figure below, and the following table enlists first year project goals:.

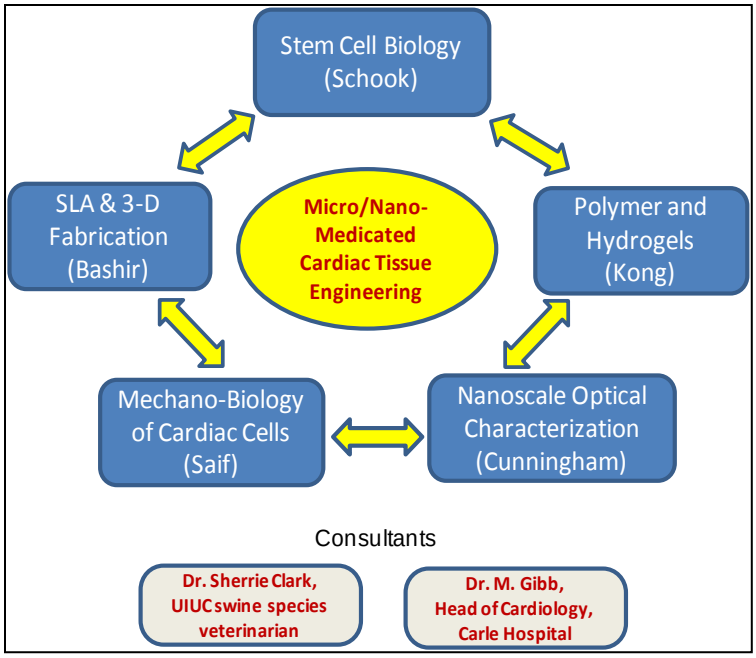

	Year 2 Project Goals
1	Demonstrate fluorescent imaging of cardiac myocytes membranes adsorbed to the photonic crystal surfaces, and selective excitation of subwavelength-sized regions from the cell surface.
2	Implement interface of nearfield scanning probe tip with a piezoelectrically controlled biosensor motion stage.
3	Culture primary chicken embryo cardiomyocytes on variable stiffness substrates. They will be mixed together with fibroblasts.
4.	Develop protocol to isolate cardiomyocytes from the chicken embryos (i.e., separate from fibroblasts).
5	Explore the molecular basis of mechanosensitivity in cardiomyocytes.
6	Demonstrate improvements of caridomyogenic differentiation level/3D cellular assembly by modulating hydrogel properties; densities of cell adhesion epitopes, mechanical stiffness/degradation rates.
7	Demonstrate fluorescent imaging of cardiac myocytes membranes adsorbed to the photonic crystal surfaces, and selective excitation of subwavelength-sized regions from the cell surface.

III. BODY

Potential Military Relevance. Battlefield trauma resulting in a variety of injuries is of significant concern to our military and civilian administration. Tissue engineering or regenerative medicine offers viable alternatives to counter many such injuries. Our project envisages to improve the care of battlefield-related cardiac injuries by providing novel methods to design and fabricate 3-D models of cardiac sub-components that would be critical in restoring the function of the heart. According to the report on 'Capturing the power of biomaterials for military medicine'(NRC Report,2004), four areas in which enhancement of biomaterials and biotechnology will have a major impact on acute, chronic, and rehabilitation care in military medicine are (1) wound care,

(2) tissue engineering, (3) drug delivery, and (4) physiological sensors and diagnostics. Our target area of research in cardiac tissue engineering, addresses one of the critical needs for the care in military medicine. The ultimate goals of our research are to resolve chronic medical problems and ultimate rehabilitation of injured military personnel (NRC Report, 2004). Our approach of using a mobilized cell population also provides flexibility in obtaining human MSCs in the field. They could be harvested from the soldiers and banked so they would have a source of their own cells. This approach is much faster and safer than bone marrow derived cells. The scaffolds we will develop could also be loaded with drugs that would be released over time to allow minimizing rejection by the body. Clearly, new methods for development of engineered tissues will have many applications beyond cardiac tissue engineering to engineering of vessels, skin, and many other organs.

IV. KEY RESEARCH ACCOMPLISHMENTS

- Cell spreading and network formation was accomplished when a degradable polymer was used for the hydrogel fabrication.
- Myoblasts were patterned using micro-contact printing and the myotube formation in 2D was examined.
- Displacement tracking has been successfully used to quantify the dynamics of myocyte culture and to explore accurately the relationship between heart shape and myocyte source *in-vitro.*
- Injectable hydrogel for the controlled release of protein drugs
- Mouse model of myocardial infarction
- Synthesize bioactive, bio-degradable methacrylic alginate (MA) and demonstrate hydrogel fabrication with stereo-lithographic apparatus.
- The methacrylic alginate-PEGDA hydrogel was combined with the SLA unit to assemble the vascularized 3D tissue engineering scaffold, which is expected to improve the cell viability and activities in a 3D matrix.
- Developed a method to characterize the permeability of hydrogel by the Magnetic Resonance Imaging (MRI)
- Designed and developed a novel strategy for making a ‘living’ microvascular stamp for neovascularization.
- Successfully monitored the growth and proliferation of several cell types, including Panc-1 pancreatic cancer cells, mouse cardiomyocytes, and HepG2 hepatic carcinoma cells
- It was shown that the biosensor can detect differences in the strength of attachment within individual cells and across different cells and to measure changes induced by exposure to drugs.

V. REPORTABLE OUTCOMES

List of Publication Accepted by Peer-Reviewed Journals

- V. Chan, P. Zorlutuna, J.H. Jeong, H. Kong, R. Bashir, Three-Dimensional Photopatterning of Hydrogels using Stereolithography for Long-Term Cell Encapsulation, Lab Chip, 2010, 10, 2062 – 2070.
- P. Zorlutuna, V. Chan, J.H. Jeong, H. Kong, R. Bashir, Long-term Viability of Cells Encapsulated in 3D Photopatterned Hydrogels Fabricated using Stereolithography, *Platform presentation*, BMES 2010 Annual meeting, October 6–9, 2010.
- V. Chan, P. Zorlutuna, J.H. Jeong, H. Kong, R. Bashir, Three-dimensional (3D) stereo-lithographic technology for bio-inspired multi-cellular structures, *Poster presentation*, BMES 2010 Annual meeting, October 6–9, 2010.
- Cha, C., Kohman, R. and Kong, H.J., Biodegradable polymer crosslinker: Independent control of stiffness, toughness, and nydrogel degradation rate. *Advanced Functional Materials* (2009) 19, 1-7
- C. Cha, S. Kim, L. Cao, H.J. Kong, "Decoupled control of stiffness and permeability of cell-encapsulated poly(ethylene glycol) hydrogel," *Biomaterials* 31, 4864-4871 (2010).

Conference Presentations

- V. Chan, P. Zorlutuna, J.H. Jeong, H. Kong, R. Bashir, 3-Dimensional Bio-Fabrication for Live Cell Encapsulation, *Platform presentation*, 6th World Congress on Biomechanics, Singapore August 1-6, 2010.

- American Institute for Chemical Engineering Nov. 8, 2010 National Meeting poster presentation: Liang, Jensen, Roy, DeVolder, Textor, Rund, Schook, Tong, Kong. Independent Control of Elasticity and Drug Release Rate of an Injectable Poly(ethylene glycol) Hydrogel for Stem Cell Mobilization.

- J.H. Jeong, V. Chan, C. Cha, Z. Pinar, R. Bashir, and H.J. Kong, “In situ Cell Encapsulation into a vascularized hydrogel matrix using a SLA.” Advances in Tissue Regenerative Symposium at UIC, Chicago (March 2010). “Awarded honorable mention.”

- J.H. Jeong, V. Chan, C. Cha, Z. Pinar, R. Bashir, and H.J. Kong, “Assembly of Vascularized Cell-Encapsulated Hydrogel Matrix using a Stereolithography.” 2010 International Conference on Biofabrication, Philadelphia (October 2010).

- J.H. Jeong, V. Chan, C. Cha, Z. Pinar, R. Bashir, and H.J. Kong, “Design of Vascularized Cell-Encapsulated Hydrogel Matrix for neovascularization.” Accepted to 2010 Materials Research Society (MRS) Fall Meeting, Boston (November 2010).

List of Manuscripts in Preparation

- Publication submitted to *Biomaterials*: Liang Y, Jensen TW, Roy EJ, Cha C, DeVolder RJ, Kohman RE, Zhang BZ, Textor KB, Rund LA, Schook LB, ong YW, Kong H. Tuning the non-equilibrium state of a drug-encapsulated super stiff poly(ethylene glycol) hydrogel for stem and progenitor cell mobilization.
- In Preparation for submission to *Xenotransplantation*: Jensen TW, Swanson DA, Rund LA, and Schook LB. An anti-porcine CD34 antibody recognizes multiple isoforms of porcine CD34.

VI. CONCLUSION

Functional 3D tissues that are designed for individual patients using multi-cellular and material compositions in an automated, high-throughput device will soon be the next generation in tissue engineering. The combination of process-optimized rapid prototyping technologies, such as stereolithography, with novel biomaterials may be one possible path toward this goal. We have shown long term cell viability, extensive cell spreading and network formation in the hydrogels fabricated with SLA. The SLA is an enabling tool with excellent spatial control and full automation capability that can potentially be used to mimic the complex 3D hierarchy of the tissue microenvironment. This may have significant impact on driving the development of *in vitro* 3D models toward broader applications, including those in tissue engineering, cell mechanics, and bio-hybrid artificial devices or multi-cellular biological machines that are capable of sensing and actuation.

Three keys aspects were investigated. First, even an apparent simple experiment such as a myocyte culture ***without*** any additional disturbance still contains far more information to be extracted than expected for something assumed to be well-known. Second: tracking the dynamics of myocytes of in-vitro experiments is a powerful strategy to correctly interpret results and to explore complex situations. The displacement myocyte gram is an easy approach with high accuracy, low to zero cost and maximal amount of data extraction. And finally, although the relationship between heart-shape and myocyte dynamics in-vitro is definitely a difficult issue, the new effects revealed in our investigations reveals the importance of bridging the gaps between full organ and cell-level mechanisms. Further investigation will have significant impact on applications to a large community of scientists involved in myocardium engineering and general heart research.

We have continued to characterize the mobilization of stem cells in the porcine model. The use of AMD3100 enables the rapid (<6 hours) mobilization of stem cells to the peripheral blood. In addition, the use of hydrogel carriers to deliver mobilization proteins can stabilize proteins and prolong their therapeutic impact in vivo. These mobilized cells have been expanded in EPC cultures and have been characterized for the expression of EPC markers in vitro and, for the first time, CD34 expression. We have also developed a small animal model of myocardial infarction that will serve as a bridging technology to test materials and reagents before moving to a more clinically relevant large animal model.

It was hypothesized that a construct capable of releasing multiple proangiogenic growth factors along a pattern engraved into that construct, while maintaining its structural integrity at the implant site, would generate the desired vascular pattern. We examined this hypothesis by encapsulating cells that were reported to endogenously express multiple proangiogenic growth factors into a rigid but permeable hydrogel of poly(ethylene glycol) (PEGDA) and methacrylic alginate (MA). In this manner, the cells were stimulated to release the soluble factors in a sustained and responsive manner. Furthermore, using a stereolithography fabrication unit, microchannels of appropriate diameter and spacing guided by Fick's law of diffusion, were incorporated into the cell-encapsulating hydrogel, so the flux of growth factors through the walls of the microchannels would be much larger than that through other parts of the hydrogel. The hydrogel permeability was evaluated by monitoring water diffusion into the hydrogel with magnetic resonance imaging (MRI), and the function of the microvascular stamp to control neovessel formation was examined by implanting it onto a chick embryo membrane (CAM).

Using this stamp, it was demonstrated that we could orchestrate the hydrogel properties and the microchannel geometry to release the cell-secreted proangiogenic factors along the circular cross-section of the microchannel and form the neovascular pattern equivalent to the pattern engraved into the stamp. Controlling the 'bottoms-up' emerging behavior of the neovessel formation via 'directed top-down' cues using the living microvascular stamp can be a major step forward in tissue engineering. We therefore propose that the resulting microvascular stamp will become a powerful tool to better understand vascular biology and also improve quality of a variety of clinical treatments necessitating the neovascularization.

We have demonstrated label-free imaging of cell attachment for a variety of cell types including panc-1, HepG2/C3 and cardiomyocytes. The instrument has the ability to monitor changes in cell adhesion over a 24-hour period at the level of individual cells, and to monitor the distinct behavior of individual cells within a population. Furthermore, we have established that he biosensor can detect differences in the strength of attachment within individual cells and across different cells and to measure changes induced by exposure to drugs. We are continuing to pursue similar studies to optimize cardiomyocyte cell culture by changing ECM components. Through the use of label-free microscopy using photonic crystal biosensors, we will gain helpful information for defining more effective cardiomyocyte culture protocols in the future.

SECTION II: Annual Report from Project Subgroups

Research Group: Rashid Bashir

Period Aug'09 to Aug'10

I. **Summary of Work**

As an overview, a commercially-available SLA was modified to accommodate for two fabrication methods: (1) the 'top-down' approach, which employs a process similar to the conventional SLA, and (2) the 'bottoms-up' approach, which allows for multiple cell types and material compositions to be arranged in their own layers within a structure (Figure 1). Laser polymerization characteristics of PEGDA hydrogels were examined and optimized for their utilization in the SLA. Complex 3D hydrogels were prepared from M_W 700 Da and fabricated in the 'bottoms-up' SLA modification (Figure 2).

II. **INTRODUCTION**

The goals of this part of the project were to assess the mechanical properties of these laser-polymerized hydrogels and evaluate the viability of cells. The swelling and mechanical properties of these hydrogels were measured as a function of M_W. Long-term viability, proliferation, and spreading of encapsulated NIH/3T3 cells over 14 days were evaluated in single-layer and multi-layer 3D structures prepared from PEGDA hydrogels with a range of M_W and RGD peptide sequences.

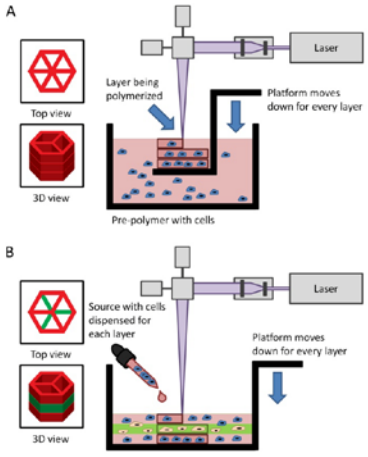

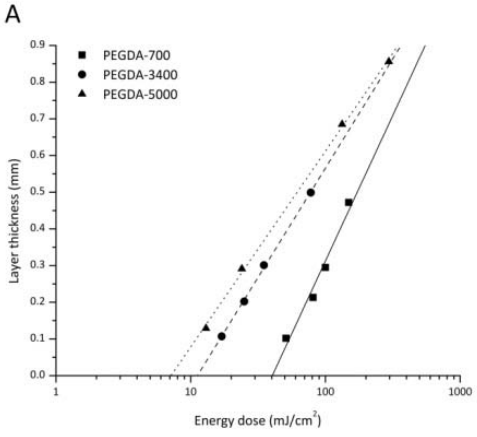

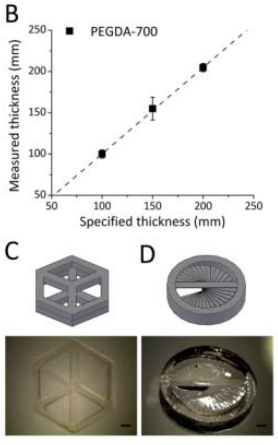

Fig. 1 (Left panel) Schematic representation of the SLA and its modification. (A) In the top-down approach, the layout consists of a platform immersed just below the surface of a large tank of pre-polymer solution. After the layer is photopolymerized, the platform is lowered a specified distance to recoat the part with a new layer. (B) In the bottoms-up approach, the pre-polymer solution is pipetted into the container one layer at a time from the bottom to the top.

Fig. 2 (Right panel) Fabrication of complex 3D hydrogels in the SLA. (A) Characterization of the laser energy dose required to cure 20% PEGDA hydrogels with M_W 700, 3,400, and 5,000 Da. (B) Example test of D_p and E_c

parameters found in (A) for M_W 700 10 Da. (C and D) CAD drawings and actual images of complex 3D hydrogels prepared from M_W 700 Da and fabricated in the bottoms-up SLA modification. All experiments used 0.5% photoinitiator concentration. Scale bars are 1 mm.

III. BODY

To demonstrate cell viability, proliferation, and spreading in biologically-relevant 3-D scaffold structures using stereolithography

Assessment of mechanical properties

The degree of swelling and the mechanical properties of laser-polymerized PEGDA hydrogels were investigated as a function of M_W. At the time of the study, the laser power of the SLA was about 15 mW and the average energy dose used to photopolymerize the gel disks was 1,600 mJ/cm^2. The swelling ratios (Q) and elastic moduli (E) for 20% (w/v) PEGDA hydrogels with M_W 700, 3,400, 5,000, and 10,000 Da were measured and calculated from these gel disks (Figure 3). As expected, the Q increased and the E decreased with increasing PEG M_W. The swelling ratios were also used to calculate the average pore size of the gel disks as a function of M_W (Table 1). The elastic moduli obtained ranged from 4.73 ± 0.46 kPa for M_W 10,000 Da to 503 ± 57 kPa for M_W 700 Da, which covers quite an array of native tissues having similar moduli. Stereomicroscopic images of PEG hydrogels after 24 hour incubation in cell culture medium showed an increase in swelling capacity with increasing M_W (Figure 4).

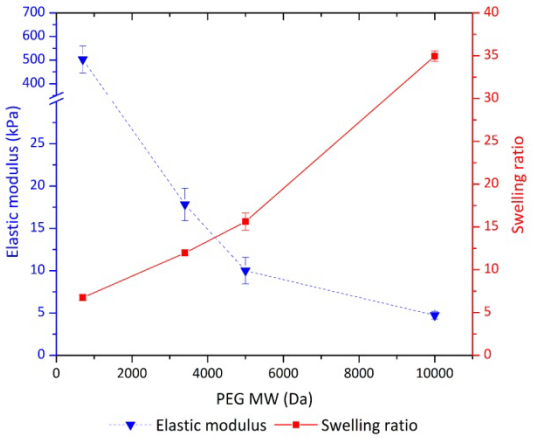

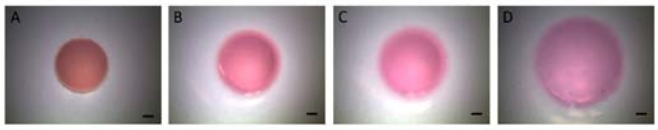

PEG M_W (Da)	Pore size (nm)
700	3.105
3,400	8.280
5,000	10.973
10,000	20.340

Fig. 3 (Left panel) Mechanical properties and swelling of laser-polymerized PEGDA hydrogels. The elastic moduli (E, left axis) and swelling ratios (Q, right axis) were measured and calculated for 20% PEGDA hydrogels as a function of M_W (700, 3,400, 5,000, and 10,000 Da). All experiments used 0.5% photoinitiator concentration.

Fig. 4 (Top right panel) Swelling of laser-polymerized PEGDA hydrogels as a function of M_W**.** 20% PEGDA hydrogels with M_W (A) 700, (B) 3,400, (C) 5,000, and (D) 10,000 Da were used to make disks with a diameter of 5 mm in the SLA. The gel disks were incubated in culture medium for 24 hours at 37^{o}C before imaging in the stereomicroscope. The diameter of the gel disks increased as a function of increasing M_W. Scale bars are 1 mm.

Table 1 (Bottom right panel) Calculated average pore sizes of laser-polymerized PEGDA hydrogels as a function of M_W. The average pore sizes of 20% PEGDA hydrogels with M_W 700, 3,400, 5,000, and 10,000 Da were calculated from values obtained by measuring the swelling ratios of gel disks with a diameter of 5 mm. The pore size increased as a function of increasing M_W.

Assessment of cell viability

There were two methods for evaluating long-term cell viability in the SLA: (1) encapsulation in single-layer 3D hydrogels (1 total layer; 1 mm thick per layer), and (2) encapsulation in multi-layer 3D hydrogels (10 total layers; 100 µm thick per layer).

In the first study, NIH/3T3 cells at a density of 2.0 X 10^6 cells/mL were encapsulated in 20% PEGDA hydrogels patterned in single-layer disks with dimensions of 1 mm thickness and 5 mm diameter. These disks were cultured over a period of 14 days. To achieve 1 mm thickness, the average energy dose of the laser during polymerization was 1,000 mJ/cm^2. Cell viability was quantitatively evaluated using MTS assays. The optical density (OD) measurements obtained from these assays on 1, 4, 7, and 14 days were converted to relative cell viability (%) by normalizing to 0 day.

The effect of a low M_W PEGDA hydrogel (700 Da) and a high M_W PEGDA hydrogel (3,400 Da) on cell viability was evaluated first (Figure 5). Cells encapsulated in PEGDA hydrogels with M_W 700 Da survived the initial processing conditions of the SLA, but died within 24 hours of culturing. By increasing the M_W to 3,400 Da, cells survived both the processing and culturing conditions. Viability remained statistically constant through 4 days. Subsequently, there was a decrease in viability to 65.10 ± 9.81 % after 7 days and to 47.46 ± 15.39 % after 14 days. Next, adhesive RGD peptide sequences at 5 mM concentration were chemically linked to PEGDA hydrogels with M_W 3,400 Da to test for any improvement in cell viability and proliferation. This resulted in a 1.6-fold increase in cell numbers after 24 hours, which was maintained over 7 days. The effect of an even greater M_W on cell viability was also evaluated (Figure 7A). Cells encapsulated in PEGDA hydrogels with M_W 5,000 Da followed the same trend as that of M_W 3,400 Da. The cell viability was relatively steady through 7 days, followed by a decrease in viability to 60.00 ± 0.2 % viability after 14 days. This was an improvement over the 14 day viability of PEGDA hydrogels with M_W 3,400 Da (47.46 ± 15.39 %).

NIH/3T3 cells encapsulated within multi-layer PEGDA hydrogels with M_W 5,000 Da were examined for cell spreading and attachment. Spreading, which involves the active processes of actin polymerization and myosin contraction, is a sign of cell viability and function. Viable cells did not spread in hydrogels without adhesive RGD peptide sequences. Cells in multi-layer PEGDA hydrogels with RGD-linked groups (5 mM) were examined in bright-field microscopy (Figures 6A and 6B) and fluorescence microscopy (Figures 6C and 6D) after rhodamine phalloidin (cytoskeleton) and DAPI (nuclei) staining. Cell spreading was clearly seen within hours of incubation and continued through 14 days. Some of these cells formed 3D connections with other cells in different layers, suggesting network formation.

Since cell viability in single-layer disks may not be truly representative of viability in complex 3D structures, the second study evaluated cells encapsulated in multi-layer 3D hydrogels over 14 days. RGD peptide sequences at 5 mM concentration were chemically linked to PEGDA with M_W 5000 Da for this

study. According to Figure 7A, the cell numbers were increased 1.7-fold after 24 hours, which was maintained through 7 days. By the end of 14 days, 46.44 ± 19.56 % of the cells were viable. Distribution of cells in single-layer and multi-layer PEGDA M_W 5000 Da hydrogels can be seen from stereomicroscopic images of hydrogels subjected to MTT staining (Figure 7B and 7C). Although there was a decrease in cell numbers after 14 days compared to 7 days, the distribution of the cells was homogeneous at both time points.

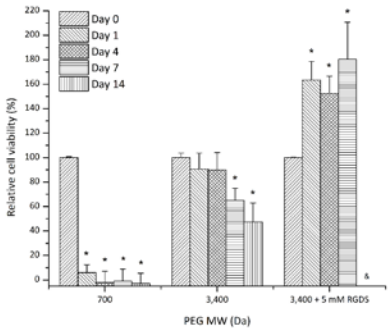

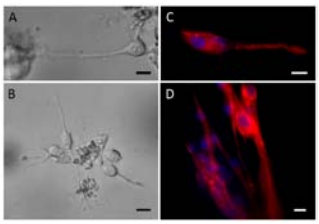

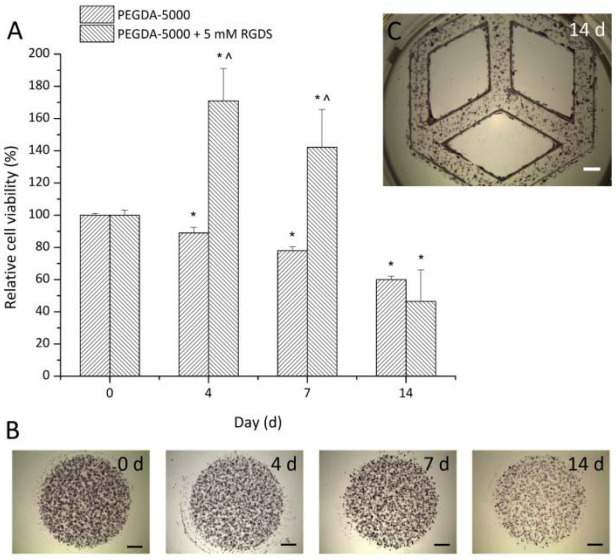

Fig. 5 (Top left panel) NIH/3T3 cell viability over 14 days in PEGDA hydrogels with M_W 700, 3,400, and 3,400 with RGDS groups. OD (490 nm) values quantified by MTS assays were normalized to 0 day. All values are mean ± standard deviation of n = 3. (*) denotes statistical difference compared to 0 day of same M_W. ($^{\&}$) denotes exclusion of data point due to uncontrolled cell proliferation at the exterior of gel disks that affected results.

Fig. 6 (Bottom left panel) NIH/3T3 cells spreading in laser-polymerized hydrogels containing bioactive RGDS groups. Single and clustered cells were clearly seen spreading in patterned multi-layer PEGDA hydrogels with M_W 5,000 Da. These hydrogels were tailored with bioactive RGDS groups at a concentration of 5 mM. (A and B) Bright-field and (C and D) fluorescence microscopy images of the cells were taken after 14 days. For fluorescence microscopy, cells were fixed and stained with rhodamine phalloidin (cytoskeleton) and DAPI (nuclei). Scale bars are 20 µm.

Fig. 7 (Right panel) NIH/3T3 cell viability over 14 days in PEGDA hydrogels with M_W 5,000 with single-layer and multi-layer approaches. (A) OD (490 nm) values quantified with MTS assay were normalized to Day 0. All values are mean ± standard deviation of n = 3. (*) denotes statistical difference compared to 0 day of same approach. ($^{\wedge}$) denotes statistical difference compared to different approach of same day. (B) MTT staining that shows living cells in a patterned multi-layer PEGDA hydrogel with M_W 5,000 Da after 14 days. (C) MTT staining that shows living cells in single-layer PEGDA hydrogel disks with M_W 5,000 Da after 0, 4, 7, and 14 days. There is a noticeable difference in intensity after 14 days. Scale bars are 1 mm.

Expanded NIH/3T3 fibroblast viability studies

To make our viability studies for NIH/3T3 fibroblasts more complete, we expanded it to include PEGDA M_W 700 and 5,000 Daltons with 5 mM RGDS. The relative cell viability trends for these two polymer

compositions followed our expectations. PEGDA M_W 700 did not support viability even with RGDS because of small average pore size and lack of oxygen/nutrient diffusion. Results for PEGDA M_W 5,000 Daltons with 5 mM RGDS indicated proliferation, which was similar to the trend for PEGDA M_W 3,400 Daltons with 5 mM RGDS.

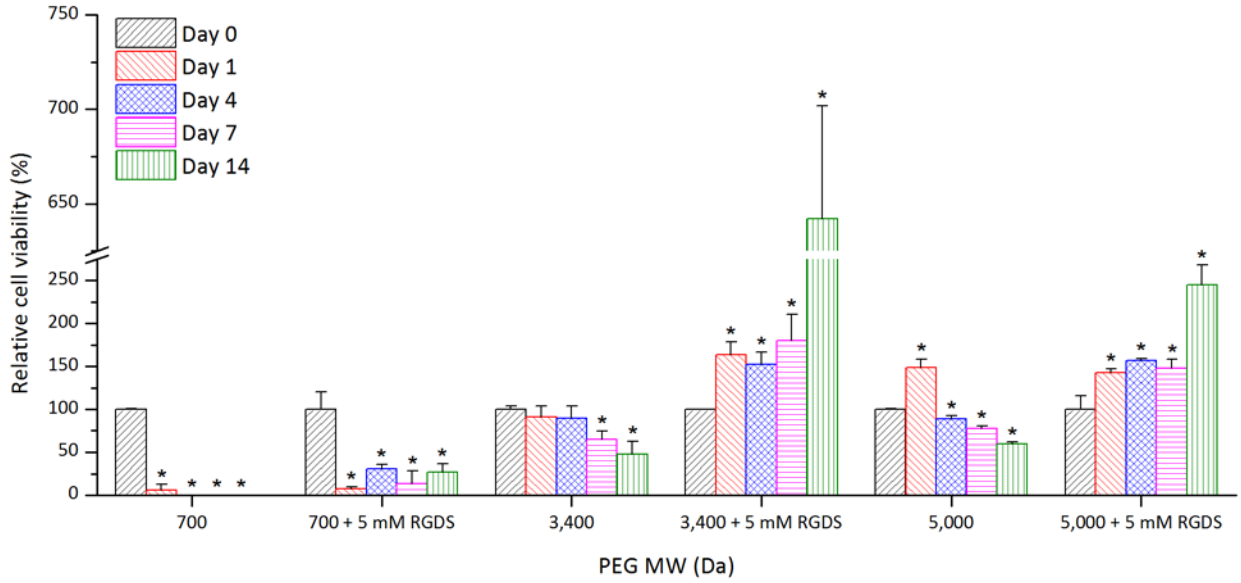

Fig. 8 NIH/3T3 cell viability over 14 days in PEGDA hydrogels with M_W 700, 3,400, and 5,000 ± RGDS groups. OD (490 nm) values quantified by MTS assays were normalized to 0 day. All values are mean ± standard deviation of n = 3. (*) denotes statistical difference compared to 0 day of same M_W.

C2C12 skeletal myoblast and adipose-derived stem cell viability studies

In an effort to expand our stereo-lithographic technology beyond fibroblasts, which are generally robust compared to other cell types, we conducted cell viability studies for C2C12 skeletal myoblasts and adipose-derived stem cells. C2C12 skeletal myoblasts in PEGDA M_W 3,400 Daltons showed a trend similar to NIH/3T3 fibroblasts, which supported viability in the hydrogels but dropped off over time. Surprisingly, we saw sustained viability for adipose-derived stem cells over 7 days before declining on the day 14. The results of these studies showed that other cell types besides fibroblasts can be encapsulated in the 3D stereo-lithographic process.

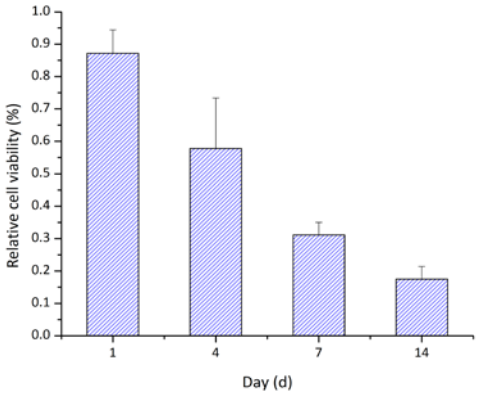

Fig. 9 C2C12 skeletal myoblasts in PEGDA M_W 3,400 Daltons. OD (490 nm) values quantified by MTS assays were normalized to 0 day. All values are mean ± standard deviation of n = 3.

Oxidized methacrylic alginate (OMA)

Synthesis of oxidized methacrylic alginate was first reported in a paper by H. J. Kong (2004). In short, alginate was oxidized with $NaIO_4$ to introduce a hydrolytically labile acetal-like unit, followed by the conjugation of 2-amino ethyl methacrylate using aqueous EDC chemistry. With the addition of PEG monoacrylate (PEGMA) and a photoinitiator, we can form a degradable hydrogel system. This is especially necessary to increase cell spreading and interaction in the gel.

The percent of oxidized groups in the methacrylic alginate affects the degradation rate of the hydrogel. Using the stereolithography apparatus, we fabricated thin gels (approx. 1 mm in thickness) and measured their elastic modulus over time. This gives us an indication of the degradation rate (% loss) based on the percent of oxidized groups.

	10% Oxidation		3% Oxidation	
Day	E (kPa)	% Loss	E (kPa)	% Loss
1	11.86 (± 1.55)	0%	8.72 (± 0.4)	0%
4	8.05 (± 0.03)	32%	6.58 (± 0.2)	25%
7	6.83 (± 0.51)	42%	5.9 (± 0.6)	32%
14	3.81	68%	5.48 (± 0.5)	37%

Table 2 Degradation rate measurements over 14 days using 10% and 3% oxidized groups of methacrylic alginate. Elastic modulus, E, values were quantified by mechanical testing system to give percent loss.

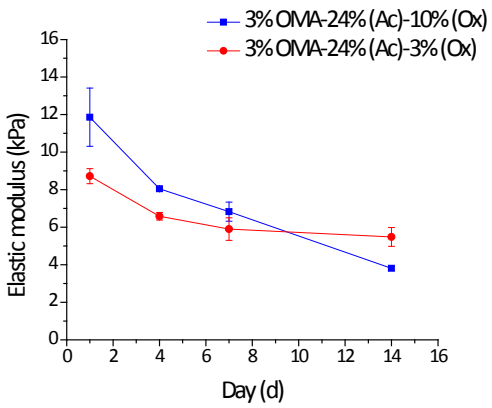

Fig. 10 Degradation rate measurements over 14 days using 10% and 3% oxidized groups of methacrylic alginate. Elastic modulus, E, values were quantified by mechanical testing system to give percent loss.

The percent of oxidized groups in the methacrylic alginate also affects the viability of cells encapsulated within the gel. This is clearly seen in the figure below. Therefore, these factors need to be considered and optimized in order to develop a suitable biomaterial for cell encapsulation within the stereolithography apparatus.

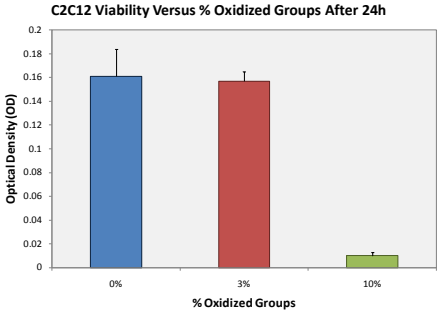

Fig. 11 Cell viability of C2C12 skeletal myoblasts in various % oxidized groups of methacrylic alginate. OD (490 nm) values quantified by MTS assays after 24 hours. All values are mean ± standard deviation of n = 3.

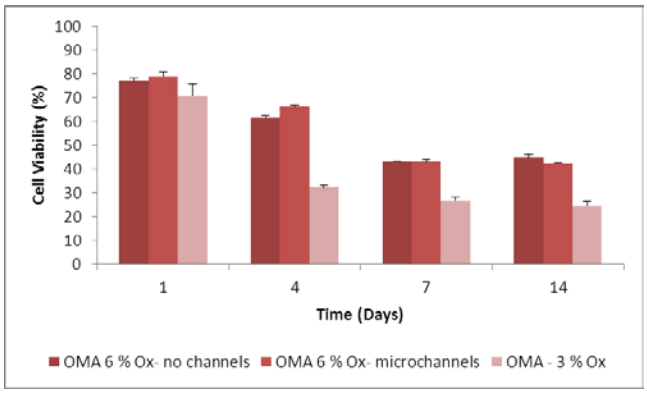

Fig 12 Cell viability of C2C12 skeletal myoblasts in various % oxidized groups of methacrylic alginate. OD (490 nm) values quantified by MTS assays for 14 days and normalized to the day 0 values. All values are mean ± standard deviation of n = 3.

After switching to a degradable polymer extensive spreading of the C2C12 cells and network formation by these cells was observed (Figure 13).

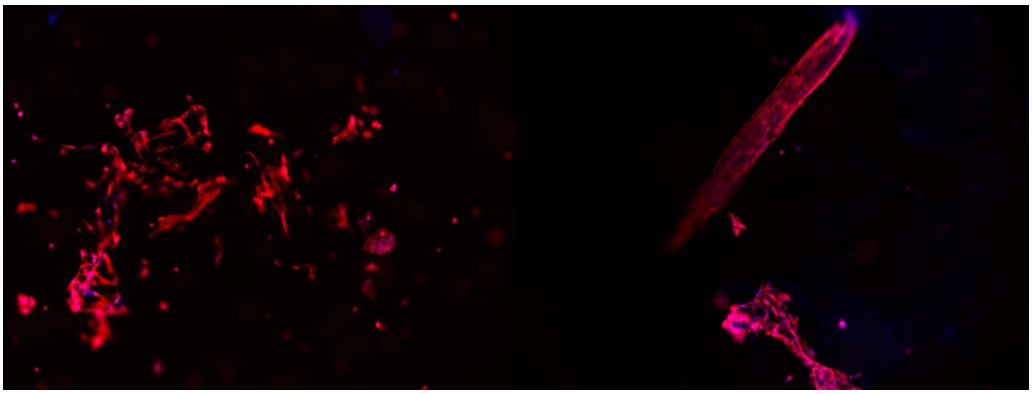

Fig 13 Fluorescent microscopy images of the C2C12s encapsulated in 6 % oxidized OMA that contains 1.6 % RGD on Day 10 of their culture. Red is Rhodamine Phalloidin for the actin cytoskeleton and blue is DAPI for the cell nuclei (Mag x 100).

NIH/3T3 fibroblast viability studies in PEGDA-MA hydrogels with and without microchannels

Previously, we have shown good cell viability in PEGDA-only hydrogels at or above M_W 3400. However, by addition of methacrylic alginate (MA), we show that we can use a lower M_W for increased elasticity and better handling without sacrificing viability. Figure 10C demonstrated that the fraction of viable NIH/3T3 cells remained similarly high with PEGDA M_W 1000 (blue bars) compared to PEGDA M_W 3400 (not shown). By using the SLA to fabricate microchannels (red bars), there is a further increase in the mass fraction of viable cells. We attributed this to the increase in mass transport through the PEGDA-MA hydrogel compared to hydrogels without microchannels.

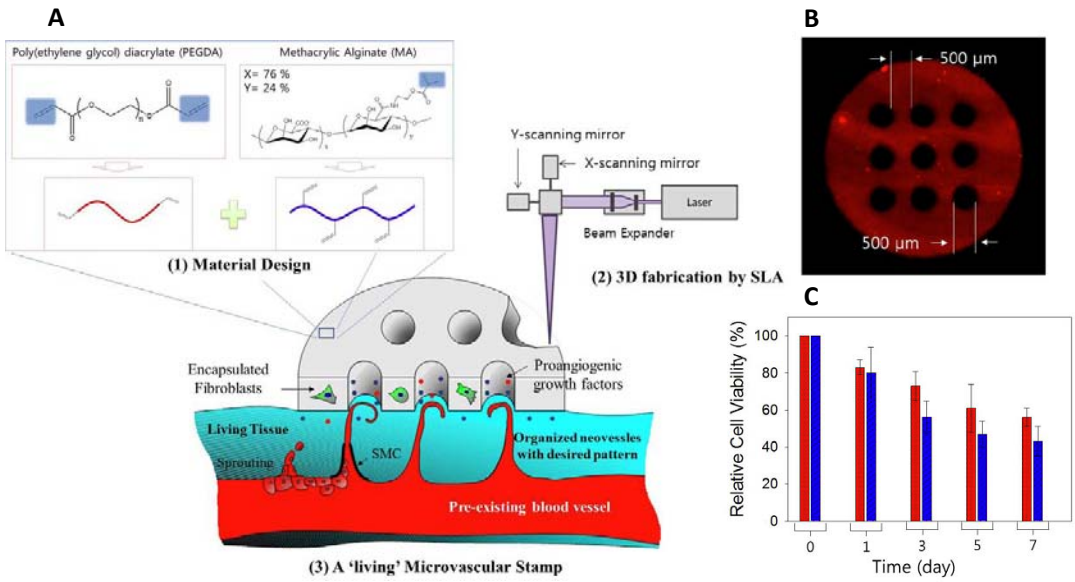

Fig. 14 (A) Schematic of the encapsulation of cells and spatial organization of microchannels within the stamp was implemented via in situ cross-linking reaction of the polymers mixed with cells using the 3-D stereolithographic (SLA) fabrication technique; **(B)** Microchannels with diameter of 500 μm were incorporated into the hydrogel via the bottoms-up process with the SLA; **(C)** The fraction of viable NIH/3T3 cells increased by introducing microchannels into the PEGDA-MA hydrogel.

2D patterning study for understanding the effect of geometry on myogenesis

Muscle fibers form from the fusion of C2C12 muscle cells into multi-nucleated myotubes. The differentiation of myoblasts to myotubes is achieved by changing the cell culture medium (10 % fetal bovine serum (FBS)) to a low serum medium (2 % horse serum) which arrests the cells mitogen activated protein kinase (MAPK) pathway leading to the development of multi-nucleated myotubes. Fig. 15A shows some fluorescent images for the differentiation of myoblasts to myotubes which was confirmed by staining for the differentiation marker – MHC (green) and nuclei are shown in blue. Fig 15B shows the differentiation index as a function of time.

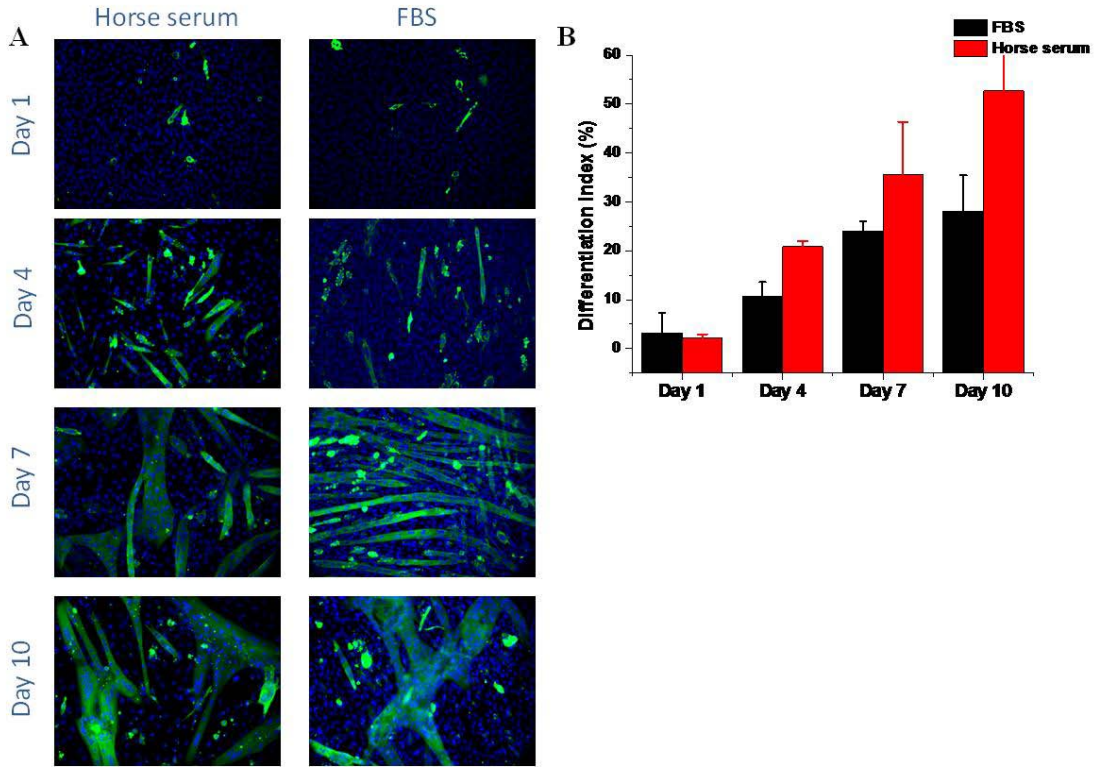

Fig 15 Differentiation of C2C12 muscle cells. (A) Fluorescent images of C2C12 muscle cells as a function of time. (B) quantification of differentiation of muscle cells into myotubes

In order to understand the effect of patterning on muscle differentiation, µCP printing was used to create protein island of different line widths. Fig. 16A shows protein island with fluorescently tagged BSA and its intensity profile. The intensity profile shows that there is very uniform concentration of BSA on each of the line widths. Cells were cultured in a similar way as in Fig. 15 and stained for MHC at different days on this protein island which is shown in Fig 16B.

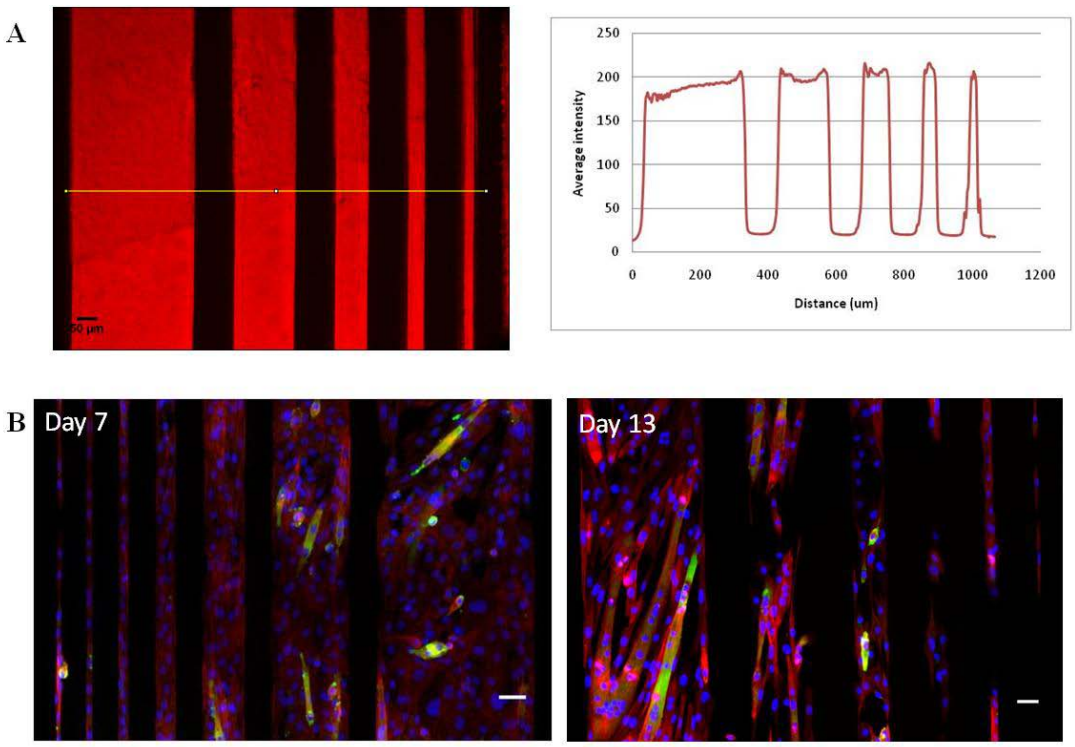

Fig 16 Patterning of C2C12 muscle cells. (A) Fluorescently tagged BSA to shown the uniformity µCP process and the fluorescent line profile. (B) C2C12 muscle cells on the protein islands on different days. Scale bar = 50 µm.

IV. KEY RESEARCH ACCOMPLISHMENTS

- Long term cell viability of different cell types were achieved using different molecular weight PEG hydrogels constructed using the SLA.
- Cell spreading and network formation was accomplished when a degradable polymer was used for the hydrogel fabrication.
- Myoblasts were patterned using micro-contact printing and the myotube formation in 2D was examined.

V. REPORTABLE OUTCOMES

- V. Chan, P. Zorlutuna, J.H. Jeong, H. Kong, R. Bashir, Three-Dimensional Photopatterning of Hydrogels using Stereolithography for Long-Term Cell Encapsulation, Lab Chip, 2010, 10, 2062 – 2070.
- P. Zorlutuna, V. Chan, J.H. Jeong, H. Kong, R. Bashir, Long-term Viability of Cells Encapsulated in 3D Photopatterned Hydrogels Fabricated using Stereolithography, *Platform presentation*, BMES 2010 Annual meeting, October 6–9, 2010.

- V. Chan, P. Zorlutuna, J.H. Jeong, H. Kong, R. Bashir, Three-dimensional (3D) stereo-lithographic technology for bio-inspired multi-cellular structures, *Poster presentation*, BMES 2010 Annual meeting, October 6–9, 2010.
- V. Chan, P. Zorlutuna, J.H. Jeong, H. Kong, R. Bashir, 3-Dimensional Bio-Fabrication for Live Cell Encapsulation, *Platform presentation*, 6th World Congress on Biomechanics, Singapore August 1-6, 2010.

VI. CONCLUSION

Functional 3D tissues that are designed for individual patients using multi-cellular and material compositions in an automated, high-throughput device will soon be the next generation in tissue engineering. The combination of process-optimized rapid prototyping technologies, such as stereolithography, with novel biomaterials may be one possible path toward this goal. We have shown long term cell viability, extensive cell spreading and network formation in the hydrogels fabricated with SLA. The SLA is an enabling tool with excellent spatial control and full automation capability that can potentially be used to mimic the complex 3D hierarchy of the tissue microenvironment. This may have significant impact on driving the development of *in vitro* 3D models toward broader applications, including those in tissue engineering, cell mechanics, and bio-hybrid artificial devices or multi-cellular biological machines that are capable of sensing and actuation.

REFERENCES

S. M. Peltola, F. P. Melchels, D. W. Grijpma and M. Kellom€aki, A review of rapid prototyping techniques for tissue engineering purposes, Ann. Med., 2008, 40(4), 268-280.

M. N. Cooke, J. P. Fisher, D. Dean, C. Rimnac and A. G. Mikos, Use of stereolithography to manufacture critical-sized 3D biodegradable scaffolds for bone ingrowth, J. Biomed. Mater. Res., 2003, 64b(2), 65–69.

B. Dhariwala, E. Hunt and T. Boland, Rapid prototyping of tissue engineering constructs, using photopolymerizable hydrogels and stereolithography, Tissue Eng., 2004, 10(9/10), 1316–1322.

K. Arcaute, B. K. Mann and R. B. Wicker, Stereolithography of three-dimensional bioactive poly(ethylene glycol) constructs with encapsulated cells, Ann. Biomed. Eng., 2006, 34(9), 1429–1441.

C. Cha, RE. Kohmon, H. Kong, Biodegradable Polymer Crosslinker: Independent Control of Stiffness, Toughness, and Hydrogel Degradation Rate Adv. Funct. Mater. 2009, 19(19), 3056-3062.

Research Group: Taher Saif

Period Oct'09 to Sept.30, 2010

I. SUMMARY OF WORK

We have shown significant differences between myocytes extracted from atrium, ventricle and apex in vitro-culture. The dynamical behavior has been observed in 4 and 6 day old myocyte cultures and quantification is proposed via computational displacement tracking of the beating cells. Our results from independent beating myocytes reveals that the ventricle myocytes "bridges" between atrium and apex. The rate of 12 bpm observed for the ventricle is similar to rate of the atrium while the amplitude of 1 μm displacement of ventricle is similar to the apex. With progressing time synchronizations occurs and the amplitudes of ventricle and apex increases by a factor of 5 while the amplitude of atrium myocytes does not change. The rate for all segments does not change within this 2 days interval. The increased amplitude with synchronization is related to the directions of contraction, also observed from a displacement myocyto gram (DMG) introduced in this investigation. These results suggest that distinguishing the source of myocytes can be crucial for bioengineering myocardium and cell transplantation therapies.

II. INTRODUCTION

Goal of this investigation:

The goals of the Taher subgroup are addressed to the community of researchers developing techniques of cell and scaffold transplantation, bioengineers constructing artificial myocardium and to general biophysicists engaged to understand and quantify fundamental relationships between myocytes in-vitro and heart behavior at entire organ level. Cells are extracted from different segments of one heart and simply observed on the petri dish without adding any external disturbance to avoid the complication of extrinsic parameters. The segments introduced are isolated parts from atrium, ventricle and apex as done in[1]. The cell culture is observed with the microscope and movies are recorded at different positions on the petri dish. From the movies a detailed analysis of cell beating is conducted based on a computational position tracking. This displacement evaluation provides not only the beating rate but also, amplitude, effects of rhythm, synchronism and time evolution relationship with cellular dynamics. In analogy to electro cardio gram (ECG) that displays the electrical activity at the full organ, a displacement myocytogram (DMG) displays the mechanical activity of the heart at the cellular level.

Is there any known relationship between heart shape and myocytes in-vitro culture?

The heart consists of different types of myocytes as they are reviewed in standard books[2]. Four decades ago, Michael M. Laks *et. al*[1] has observed myocytes from different places of the heart

with distinguished cell and sarcomere length. In the abstract of his publication he clearly emphasized with the following words: >>*… these variations on sarcomere lengths show the importance on specifying the site of sampling of myocardial tissue…*<< At the full organ level, the shape of the heart is frequently brought in relationship with disease. In particular the left ventricle is responsible for several heart diseases and is mostly studied in recent years[3-9]. Since last decade cell transplantation[10-20], scaffold injection[21-31] and bioengineered myocardium tissues[32-44] have been recognized as potential candidates for repairing heart failure. However, meanwhile little attention has been given to the source of myocytes.

What is the shape of the heart causing in scientific studies at the entire organ level?

Pacing at the right ventricular apex adversely affects hemodynamics while pacing at the left ventricular septum or apex causes best function because pacing from these sites creates a physiological propagation of electrical conduction[3]. Right and left apex has been distinguished by increase of its surface area and relative cell alignment during heart looping[45]. Atrial and ventricle myocardium have shown different mechanism of force generation in response to external stretching[46] and electromechanically coupling demonstrated that increase force of contraction following an increase in frequency stimulation was significantly higher in atrium than in ventricle[47]. Epicardium and endocardium of left ventricular tissues have shown the importance of regional structures on amplifying fiber shortening, to produce wall thickening, to provoke different alignment during contraction and cellular rearrangements are also different at the 2 sites[48, 49] In obese patients increase of left ventricle mass exceeds the compensation of high hemodynamic load and is associated with mildly reduced left ventricular myocardial performance and increased left atrial force to contribute to left ventricle filling[50].

III. BODY

1.1 Extraction of the heart and cell culture

Cardiomyocytes were obtained from 5-day old neonatal Sprague-Dawley rats (Harlan Laboratories, Inc.) using an approved protocol by the Institutional Animal Care and Use Committee (IACUC; Protocol #08190). One heart was excised from the rat as described by AH Maass and M Buvoli[51, 52] and placed in ice-cold HBSS buffer.

1.2 Segments of different parts of the heart

The two heart chambers were separated immediately after killing the rat. It was easier to cut the heart while it was still beating and involved by the lungs because in this way the dark color of the right ventricle was obvious and one can cut ***along*** the inter ventricular septum as shown in Figure 1b. On the other hand, if the heart was cut ***across*** the septum, each chamber is separated by the septum and both right and left ventricular walls can be seen in one half of the heart. In this investigation, only the left atrium, left ventricle and left apex were used.

A micro digital camera was mounted inside the sterilized hood to precisely cut the segments of the heart. The camera, Dnt Mikroskopkamera Digimicro 2.0 Scale, had a large working distance

and a practical magnification of 20x. The segmentation was monitored outside the hood using a computer screen. The procedure above is unavoidable to cut segments of equal sizes which are necessary to obtain similar cell concentrations for a given volume of cell suspension at the end of the cell extraction. Screen monitoring is also helpful to precisely identify the apex, the ventricle and the atrium and to reproduce the segmentation of different hearts. The left part of the heart was cut in 5 pieces (Figure 1c) because only three of them (1, 3 and 5) were used to extract the cells while the segments 2 and 4 are waist. The exclusion of 2 and 4 were necessary to obtain accurate isolation of each segment without containing cells of its neighborhood. Compared to the segmentations discussed in[12, 18, 22, 53], here is noticed that the healthy tissue were cut for cell extraction and cell culture of these segments is the subject of observation. Furthermore, in this investigation were used only hearts of female rats because they beat faster than male ones as shown in[54, 55]. Mixture of hearts from many rats was not taken in consideration because each heart can lead to different beating rates as it has been observed in preliminary experiments in this lab with the full organ (results not shown). The typical concentration all cell-culture was roughly 4-5 cells per 400μm^2.

1.3 Image analysis and dynamical behavior of myocytes via matlab

In this project we introduced a displacement myocytogram (DMG). It is a two dimensional position tracking of the beating of one myocyte with the used of Matlab. The tracked position is one pixel marked at a clearly visible moving boundary, typically at the cell membrane. The position includes the surrounding region of that pixel, technically named correlation size. The correlation size is determined according to the amplitude of the displacement and depends on the individual properties of each dynamical event. If the selected position changes its coordinates in series of images extracted from a movie, one can extract the coordinates as a function of time, display the displacements and follow the dynamical behavior of that point. Figure 2 displays a validation of the method. The quality of the movie and displacement tracking is tested based on the oscillation of a metronome where frequency and amplitude are fixed and known.

The cell beating is followed in all directions by selection of more than one position along the cell membrane. The complete movement is reconstructed by combining all displacement versus time (displacement myocytogram, “DMG”) of one myocyte in all directions of motion. The method above has been validated in this lab by tracking the position of an oscillating metronome with defined frequencies and amplitudes. Matlab has been used also in previous studies[56-58] for image processing and demonstrated high accurate results. A future publication with emphasis on the methods including the validation is on preparation for submission.

2.1-Independent dynamical behavior of myocytes (Displacement Myocytogram – DMG)

Comparing myocytes from different segments:

In Figure 3a-c is displayed the membrane displacement versus time of beating myocytes from different segments of the heart. Atrium-Ventricle: Comparing the DMG behavior between atrium and ventricle in terms of frequency demonstrates similar to identical rate of 12-13 beats per minute. However, additional to the frequency it is clearly observed an amplitude reduction in the

ventricle by half the amplitude of the atrium. Furthermore, the regular frequency of the atrium is not observable for the ventricle which displays certain arrhythmic dynamic. Ventricle-apex: Further comparison between ventricle and apex shows a new difference: while their amplitudes are similar and approaching 0.8 μm, their frequencies are different. The apex beats additional five times per minute. It is interesting to observe that although the number of cells counted for the apex is the largest, the near perfect synchronism is found in the atrium. *Atrium-apex:* Comparison between atrium and apex lead to absolutely distinguishable behavior at the cellular level.

Statistical characteristics

In the following is presented the rate of beating cells for the apex, ventricle and atrium. Five movies were recorded in positions about 3 mm apart from each other from a segment culture. The same procedure applies for the videos of the other segments. The statistic evaluation from the analysis of all videos and number of cells of the videos is listed below:

Table 1. Statistical results for the rate of beating cells from different segments of the heart.

Segment	**Apex**	**Ventricle**	**Atrium**
Number of cells	49	31	22
Average	17.69	11.09	11.86
Stand. Deviation	3.083	1.325	0.833
Mean Deviation	2.071	1.073	0.706

Following the values on the table above is observed that the cells of apex beat the fastest while cells from ventricle and atrium do not distinguish significantly. Since the number of cells counted for the apex is largest, also the density of cells per unit area is higher in this sector. The consequence of cell density and beating rate will be discussed below.

2.2 Collective behavior

Two days after the experiments above, new series of movies were recorded in the same way as above and the resulted DMGs are displayed in Figure 4a-c.

Amplitude: Interestingly, short time was sufficient to connect most of the cells and new scenario build up. The frequency did not change and the values conserved their earlier rate. About 16 cells were observed and the graphs presented in Figure represent typical scenarios. The records for the amplitude surprised with values 5 times larger than in the previous experiment for non-connected cells. But this increased amplitude from 1 μm to about 5 μm was found only for the apex and ventricle while the amplitude of the atrium slightly reduced from 2μm to about 1.7 μm.

Rhythm: In the previous experiment, except the atrium, myocytes from apex and ventricle were beating without well-defined rhythm. Here is briefly emphasized on the difference between intrinsic rhythm of *one* cell and beating in synchrony with other cells. Using a comparison

between the results of these two experiments: 1) the atrium had one rhythm before and after cell-cell connection, basically, a cell can beat alone but with one frequency. This does not happen for the apex and ventricle. Both of them had more than one frequency in the prior experiment and the number of different frequencies only reduced in the second situation. 2) Although multiple myocyte are interconnected, they are not necessarily beating with the same frequency. For reasons of different force distribution their amplitude increased, but not due to intrinsic rhythym.

Synchronism: It is definitely valid to state that two absolutely synchronized myocytes will have identical frequencies, but the fact that there is more than one frequency shows that there is more than one rhythm. In summary: synchronism does not implicate one rhythmus but surely if there is one rhythmus between more than one beating myocytes, they are necessarily synchronized.

3.1 Limitations of standard analysis and advantages of introduced method

The limit of human observation

Tracking displacements via Matlab becomes a powerful tool to display unseen events because eyes cannot always follow every change of a movement. The effect of amplitude increase with synchronization is one among other examples of what can be achieved with detailed analysis.

3.2 What DMG brings new? Is a displacement analysis really necessary?

Physical properties of dynamical events

The full mechanical quantities of any dynamical event are in general vectors because motion implicates direction and velocity. To use a scalar number to quantify the frequency of a myocyte is an interesting approach, however it is noticed that analysis based on the rate per minute alone occurs under suppression of the instantaneous velocity, direction and amplitude of momentum. The instantaneous velocity tells one, for example, if a cell behavior is perfectly cyclic along time or if the cell stops beating for a moment and beat twice in the next period. Following this thought, one can measure, for example, one frequency between two distinguishable cells moving with different dynamical behavior, such as an arrhythmic and another perfectly cyclic beating cell. A result like that implicates that a direct comparison between these two events might not be necessarily fair and would lead to wrong conclusion. In such situation, although the frequency would be identical, the arrhythmia of one cell could be an indicator of an unhealthy state. Additional to the information contained in the velocity, the direction of beating sometimes also changes responding either to local changes of chemical or mechanical stimulus. This information likewise is lost in the scalar frequency and could be missed for understanding local effects, such as force transduction measurement.

3.3 Effect of heart segments

Time evolution and aging of cell culture

Apparently there are important trends observed for the correlation between heart geometry at the cellular behavior. However, since this observation was performed at the fourth and sixth day, it is necessary to carefully consider the time evolution in this discussion. The fact that the standard and mean deviation is negligibly small as shown in Table 1, though the number of cells is large; it is an indicator that cell synchronization is occurring. Based on this assumption, the arrhythmic ventricle compared to the regular beating atrium in Figure 5a-b might have less to do with heart segments, and more with an effect due to higher advanced state of synchronism of atrium relative to the ventricle.

Synchronization, amplitude increase and co versus contra cooperative interaction

Geometrical effect on myocyte culture seems to increase its importance in the context of age of myocyte culture. The 5 times higher amplitudes observed in Figure 4 is difficult to be addressed to synchronism alone. They could have been synchronized even 2 days earlier as shown in Figure 3, nevertheless, it maximal amplitude was about 2 microns and it conserved near the same value 2 days later. Thus, why only the values of amplitude for apex and ventricle increased? These facts lead to the next question on the mechanism occurring during synchronization. Is synchronism an effect of heart geometry or fibroblast connection alones resolves the problem and would not depend on the source of cell? This question is difficult to answer and additional studies are needed to address this problem.

Similarity between full organ and myocyte dynamics and clinical relevance of the present study:

The similar behavior for near segments can be found at both cellular and full organ level, such as the frequency between atrium and ventricle and the amplitude between ventricle and atrium but no relationship found between apex and atrium. This relationship might reflect the spatial separation between apex and atrium and the proximity of the ventricle to each of them. The increase of amplitude for the apex and ventricle of the beating myocytes is another property with similarity at the full organ level, since the ventricle is squeezing the blood out of the chamber and while the atrium “helps” during inner flow. Since increase of amplitude as response to synchronism is a measure of contraction and dilation, this event can be reasonably correlated to wall thickening of ventricular walls. Wall thickening exceed values of 40% while shortening of individual myocytes is being reported to be 15%[48, 49]. If the increase of amplitude by a factor of 5 reported would be directly translated to wall thickening, the value would even be larger than the clinical. However, the in-vitro myocytes observed here are not working against an external pressure. Further studies in this relationship could have potential impact in bioengineered myocardium. Future studies of time evolution of mechanical behavior of myocytes from different segments of the heart in long ranged cell culture can be beneficial for bridging geometric effects between cellular and full organ, such as to answer why the analysis of left ventricle geometry different patients reveals concentric hypertrophy in about 49%, concentric remodeling in 24% and eccentric hypertrophy in 12% of the studied patients[6].

IV. KEY RESEARCH ACCOMPLISHMENTS

- Displacement tracking has been successfully used to quantify the dynamics of myocyte culture and to explore accurately the relationship between heart shape and myocyte source in-vitro.
- The origin of myocytes makes significant differences in the dynamics of beating and reveals the importance of further studies to evaluate the implications on bioengineering myocardium.

V. REPORTABLE OUTCOMES (papers in preparation)

- How myocytes from different segments of the heart differs in the cell culture? A physical point of view.
- Fibroblastation and synchronization: The cell coupling paradigm quantified via vector field analysis.
- From tracking one beating myocyte to mapping a field of myocytes: A method for quantification of dynamical fields.

VI. CONCLUSION

Three keys messages were presented in this manuscript: First, even an apparent simple experiment such as a myocyte culture ***without*** any additional disturbance still contains far more information to be extracted than expected for something assumed to be well-known. Second: tracking the dynamics of myocytes of in-vitro experiments is a powerful strategy to correctly interpret results and to explore complex situations. The displacement myocyto gram is an easy approach with high accuracy, low to zero cost and maximal amount of data extraction. And finally, although the relationship between heart-shape and myocyte dynamics in-vitro is definitely a difficult issue, the new effects revealed in our investigations reveals the importance of bridging the gaps between full organ and cell-level mechanisms. Further investigation will have significant impact on applications of large community of scientists involved on myocardium engineering and general heart research.

VII. REFERENCES

1. Laks MM, Nisenson MJ, Swan HJ. Myocardial cell and sarcomere lengths in the normal dog heart. *Circulation Research*. 1967;21:671-678
2. Opie LH. Heart cells and organelles. In: Opie LH, ed. *Heart physiology: From cell to circulation*. Philadelphia: Lippincott Williams & Wilkins; 2004:42-69.
3. Peschar M. Left ventricular septal and apex pacing for optimal pump function in canine hearts. *Journal of the American College of Cardiology*. 2003;41:1218-1226
4. Storaa C. Tissue motion imaging of the left ventricle - quantification of myocardial strain, velocity, acceleration and displacement in a single image. *European journal of echocardiography*. 2004;5:375-385

5. Ricci E, Smallwood S, Chouabe C, Mertani HC, Raccurt M, Morel G, Bonvallet R. Electrophysiological characterization of left ventricular myocytes from obese sprague-dawley rat. *Obesity*. 2006;14:778-786
6. Hare JL, Brown JK, Marwick TH. Association of myocardial strain with left ventricular geometry and progression of hypertensive heart disease. *American Journal of Cardiology*. 2008;102:87-91
7. Miyachi M, Yazawa H, Furukawa M, Tsuboi K, Ohtake M, Nishizawa T, Hashimoto K, Yokoi T, Kojima T, Murate T, Yokota M, Murohara T, Koike Y, Nagata K. Exercise training alters left ventricular geometry and attenuates heart failure in dahl salt-sensitive hypertensive rats. *Hypertension*. 2009;53:701-707
8. Uchino K, Ishigami T, Ohshige K, Sugano T, Ishikawa T, Kimura K, Umemura S. Left ventricular geometry, risk factors, and outcomes of hospitalized patients with diastolic heart failure in japan. *Journal of Cardiology*. 2009;54:101-107
9. Roman MJ, Okin PM, Kizer JR, Lee ET, Howard BV, Devereux RB. Relations of central and brachial blood pressure to left ventricular hypertrophy and geometry: The strong heart study. *Journal of Hypertension*. 2010;28:384-388
10. Taylor DA, Atkins BZ, Hungspreugs P, Jones TR, Reedy MC, Hutcheson KA, Glower DD, Kraus WE. Regenerating functional myocardium: Improved performance after skeletal myoblast transplantation. *Nature Medicine*. 1998;4:929-933
11. Hutcheson KA, Atkins BZ, Hueman MT, Hopkins MB, Glover DD, Taylor DA. Comparison of benefits on myocardial performance of cellular cardiomyoplasty with skeletal myoblasts and fibroblasts. *Cell transplantation*. 2000;9:359-368
12. Muller-Ehmsen J. Rebuilding a damaged heart: Long-term survival of transplanted neonatal rat cardiomyocytes after myocardial infarction and effect on cardiac function. *Circulation*. 2002;105:1720-1726
13. Taylor DA. Is in vivo remodeling necessary or sufficient for cellular repair of the heart? *Reparative Medicine: Growing Tissues and Organs*. 2002;961:315-318
14. Thompson RB, Parsa CJ, van den Bos EJ, Davis BH, Toloza EM, Klem I, Glower DD, Taylor DA. Video-assisted thoracoscopic transplantation of myoblasts into the heart. *Annals of Thoracic Surgery*. 2004;78:303-307
15. van den Bos EJ, Davis BH, Taylor DA. Transplantation of skeletal myoblasts for cardiac repair. *Journal of Heart and Lung Transplantation*. 2004;23:1217-1227
16. Murry CE. Cell-based cardiac repair reflections at the 10-year point. *Circulation*. 2005;112:3174-3183
17. Ott HC, Taylor DA. From cardiac repair to cardiac regeneration - ready to translate? *Expert Opinion on Biological Therapy*. 2006;6:867-878
18. Zimmermann WH, Didié M, Döker S, Melnychenko I, Naito H, Rogge C, Tiburcy M, Eschenhagen T. Heart muscle engineering: An update on cardiac muscle replacement therapy. *Cardiovascular research*. 2006;71:419-429
19. Laflamme MA, Chen KY, Naumova AV, Muskheli V, Fugate JA, Dupras SK, Reinecke H, Xu C, Hassanipour M, Police S, O'Sullivan C, Collins L, Chen Y, Minami E, Gill EA, Ueno S, Yuan C, Gold J, Murry CE. Cardiomyocytes derived from human embryonic

stem cells in pro-survival factors enhance function of infarcted rat hearts. *Nature Biotechnology*. 2007;25:1015-1024

20. Sun CK, Chang LT, Sheu JJ, Chiang CH, Lee FY, Wu CJ, Chua S, Fu M, Yip HK. Bone marrow-derived mononuclear cell therapy alleviates left ventricular remodeling and improves heart function in rat-dilated cardiomyopathy. *Critical Care Medicine*. 2009;37:1197-1205
21. Leor J. Bioengineered cardiac grafts: A new approach to repair the infarcted myocardium? *Circulation*. 2000;102:III56-III61
22. Christman KL, Fok HH, Sievers RE, Fang Q, Lee RJ. Fibrin glue alone and skeletal myoblasts in a fibrin scaffold preserve cardiac function after myocardial infarction. *Tissue Engineering*. 2004;10:403-409
23. Christman KL, Vardanian AJ, Fang Q, Sievers RE, Fok HH, Lee RJ. Injectable fibrin scaffold improves cell transplant survival, reduces infarct expansion, and induces neovasculature formation in ischemic myocardium. *Journal of the American College of Cardiology*. 2004;44:654-660
24. Rittman L, Vesely I. Novel geometries for collagen constructs applied to tissue-engineered heart valves. 2004:440
25. Dai W, Wold LE, Dow JS, Kloner RA. Thickening of the infarcted wall by collagen injection improves left ventricular function in rats: A novel approach to preserve cardiac function after myocardial infarction. *Journal of the American College of Cardiology*. 2005;46:714-719
26. Gilbert TW. Decellularization of tissues and organs. *Biomaterials*. 2006;27:3675-3683
27. Suuronen EJ, Veinot JP, Wong S, Kapila V, Price J, Griffith M, Mesana TG, Ruel M. Tissue-engineered injectable collagen-based matrices for improved cell delivery and vascularization of ischemic tissue using cd133+progenitors expanded from the peripheral blood. *Circulation*. 2006;114:I138-I144
28. Badylak SF. The extracellular matrix as a biologic scaffold material. *Biomaterials*. 2007;28:3587-3593
29. Ott HC, Matthiesen TS, Goh SK, Black LD, Kren SM, Netoff TI, Taylor DA. Perfusion-decellularized matrix: Using nature's platform to engineer a bioartificial heart. *Nature Medicine*. 2008;14:213-221
30. Singelyn JM. Naturally derived myocardial matrix as an injectable scaffold for cardiac tissue engineering. *Biomaterials*. 2009;30:5409-5416
31. Singelyn JM, DeQuach JA, Christman KL. Injectable myocardial matrix as a scaffold for myocardial tissue engineering. 2009:2406-2408
32. Zimmermann WH, Eschenhagen T. Cardiac tissue engineering for replacement therapy. *Heart Failure Reviews*. 2003;8:259-269
33. Radisic M. Functional assembly of engineered myocardium by electrical stimulation of cardiac myocytes cultured on scaffolds. *Proceedings of the National Academy of Sciences of the United States of America*. 2004;101:18129-18134
34. Zimmermann WH, Melnychenko I, Eschenhagen T. Engineered heart tissue for regeneration of diseased hearts. *Biomaterials*. 2004;25:1639-1647

35. Eschenhagen T, Zimmermann WH. Engineering myocardial tissue. *Circulation research*. 2005;97:1220-1231
36. Lutolf MP, Hubbell JA. Synthetic biomaterials as instructive extracellular microenvironments for morphogenesis in tissue engineering. *Nature Biotechnology*. 2005;23:47-55
37. Gerecht-Nir S. Biophysical regulation during cardiac development and application to tissue engineering. *The international journal of developmental biology*. 2006;50:233-243
38. Zimmermann WH. Engineered heart tissue grafts improve systolic and diastolic function in infarcted rat hearts. *Nature Medicine*. 2006;12:452-458
39. Adams WJ, Pong T, Geisse NA, Sheehy SP, Diop-Frimpong B, Parker KK. Engineering design of a cardiac myocyte. *Journal of Computer-Aided Materials Design*. 2007;14:19-29
40. Cannizzaro C, Tandon N, Figallo E, Park H, Gerecht S, Radisic M, Elvassore N, Vunjak-Novakovic G. Practical aspects of cardiac tissue engineering with electrical stimulation. In: Hauser H, Fussenegger M, eds. *Methods in molecular medicine: Tissue engineering*. Totowa, New Jersey: Humana Press Inc.; 2007:291-307.
41. Geisse NA. Control of myocyte remodeling in vitro with engineered substrates. *In Vitro Cellular & Developmental Biology; Animal*. 2009;45:343-350
42. Reing JE, Zhang L, Myers-Irvin J, Cordero KE, Freytes DO, Heber-Katz E, Bedelbaeva K, McIntosh D, Dewilde A, Braunhut SJ, Badylak SF. Degradation products of extracellular matrix affect cell migration and proliferation. *Tissue Engineering - Part A*. 2009;15:605-614
43. Alford PW, Feinberg AW, Sheehy SP, Parker KK. Biohybrid thin films for measuring contractility in engineered cardiovascular muscle. *Biomaterials*. 2010;31:3613-3621
44. Hosoda T. Mechanisms of myocardial regeneration. *Circulation journal : official journal of the Japanese Circulation Society*. 2010;74:13-17
45. Manasek FJ, Burnside MB, Waterman RE. Myocardial cell shape change as a mechanism of embryonic heart looping. *Developmental Biology*. 1972;29:349-371
46. Kockskämper J, von Lewinski D, Khafaga M, Elgner A, Grimm M, Eschenhagen T, Gottlieb PA, Sachs F, Pieske B. The slow force response to stretch in atrial and ventricular myocardium from human heart: Functional relevance and subcellular mechanisms. *Progress in Biophysics and Molecular Biology*. 2008;97:250-267
47. Schwinger RHG. Force-frequency-relation in human atrial and ventricular myocardium. *Molecular and cellular biochemistry*. 1993;119:73-78
48. Cheng A, Nguyen TC, Malinowski M, Daughters GT, Miller DC, Ingels Jr NB. Heterogeneity of left ventricular wall thickening mechanisms. *Circulation*. 2008;118:713-721
49. Covell JW. Tissue structure and ventricular wall mechanics. *Circulation*. 2008;118:699-701
50. Chinali M, de Simone G, Roman MJ, Lee ET, Best LG, Howard BV, Devereux RB. Impact of obesity on cardiac geometry and function in a population of adolescents. The strong heart study. *Journal of the American College of Cardiology*. 2006;47:2267-2273

51. Maass AH, Buvoli M. Cardiomyocyte preparation, culture, and gene transfer. In: Zhang J, Rokosh G, eds. *Methods in molecular biology, cardiac gene expression: Methods and protocols*. Totowa, New Jersey: Humana Press Inc.; 2007:321-330.
52. Chlopcíková S, Psotová J, Miketová P. Neonatal rat cardiomyocytes--a model for the study of morphological, biochemical and electrophysiological characteristics of the heart. *Biomedical papers of the Medical Faculty of the University Palacky, Olomouc, Czechoslovakia*. 2001;145:49-55
53. Li RK. Cardiomyocyte transplantation improves heart function. *The Annals of thoracic surgery*. 1996;62:654-661
54. Buñag RD, Davidow LW. Aging impairs heart rate reflexes earlier in female than in male sprague-dawley rats. *Neurobiology of Aging*. 1996;17:87-93
55. Stupfel M, Costagliola D. Lifelong variations in heart rates in spf sprague dawley rats of both sexes. Statistical correlations with body weights. *Pflugers Archiv European Journal of Physiology*. 1979;380:189-195
56. Zuria CS, Ramirez JM, Baez-Lopez D, Flores-Verdad GE. Matlab based image processing lab experiments. 1998;3:1255-1258
57. Chacon MI. Fast image processing application development scheme for the dsk c6711 using matlab and simulink. *2004 IEEE 11th Digital Signal Processing Workshop and 2nd IEEE Signal Processing Education Workshop*. 2004:79-83
58. Bister M. Increasing the speed of medical image processing in matlab®. *Biomedical imaging and intervention journal*. 2007;3

Figures

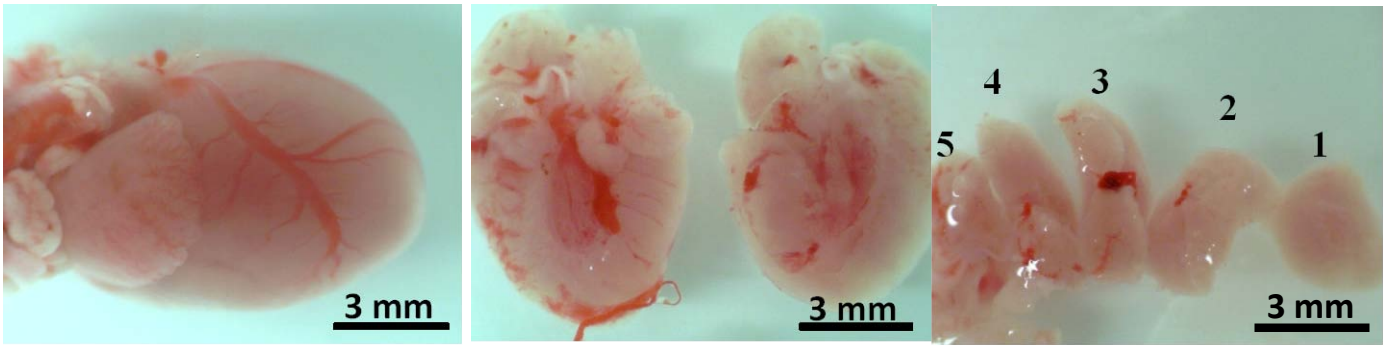

(a) **(b)** **(c)**

Figure 1 (a) Image of the entire heart in HBSS at 4°C 20 min. after dissection and before segmentation. **(b)** Cut of the heart along the inter-ventricular septum, the left and right are exposed. Both atriums are not visible because the vascular tissues glued to the chambers. **(c)** Final segmentation of the left chamber before used for trypsin digestion and cell extraction. From left to right: atrium (5), extra tissue (4), ventricle (3), extra tissue (2) and apex (1). The extra tissues are not used for cell culture.

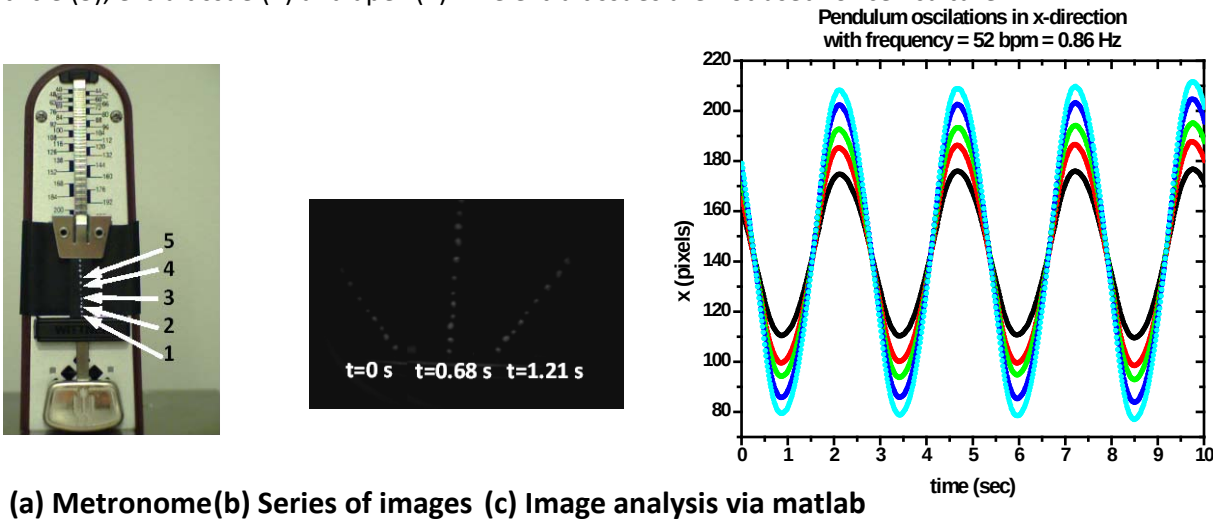

(a) Metronome(b) Series of images (c) Image analysis via matlab

Figure 2 (a) Experimental set up to record displacements of dots oscillating with rates ranging from 40 to 208 beats per minute (bmp) and at different amplitudes which are fixed by the height of the dots, each separated by approximately 1mm. **(b)** Series of images extracted from a movie recorded with 60 frames per second and metronome frequency fixed to 52 bpm. **(c)** Evaluation of displacements tracking Matlab. The amplitude of the oscillation in x-direction increases as the observed point in the metronome changes from bottom (p1) to top (p5), assigned with the colors black to cyan, respectively

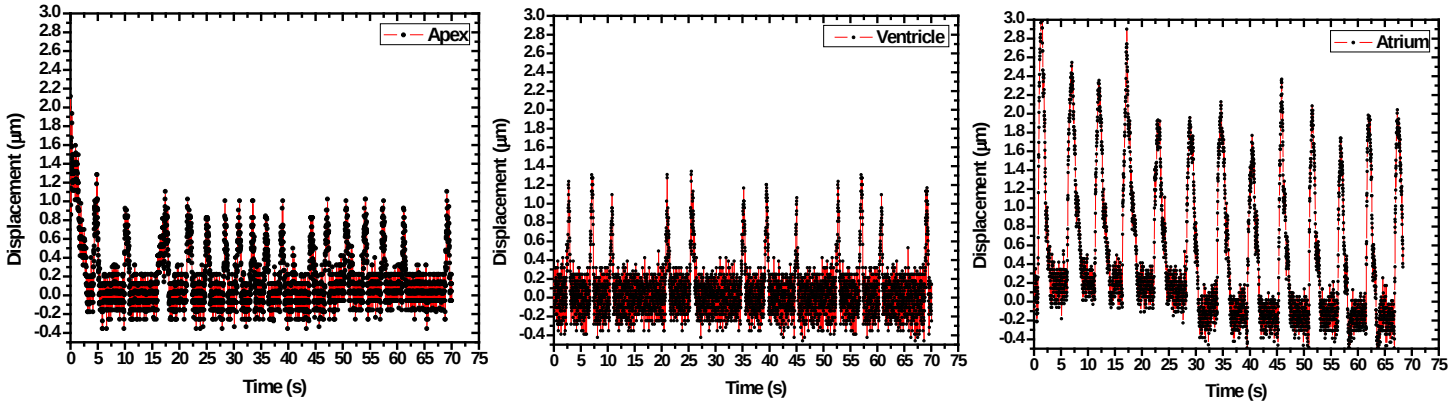

(a) (b) (c)

Figure3 (a-c) Displacement myocyto gram (DMG) of beating myocytes. It is the tracking of movement or displacement at the membrane of one cell. Each graph displays the beating at the position of the membrane with highest amplitude. Thus, a DMG reflects the dynamical behavior of a myocyte in vitro. The graphs **(a)** apex, **(b)** ventricle and **(c)** atrium are obtained from a 4 days old culture on petri dish. The myocytes in each video are beating independent of its neighborhood without any apparent mechanical connection. Cells on apex and ventricle have similar amplitude of approximately 1.275µm but different beating rate. The rate of apex is 17 bpm and of ventricle 12 bpm. On the other hand, cells on ventricle and atrium have the same beating rate but different amplites. The amplitude of atrium is approximately double the amplitude elsewhere. Consequently, no relationship can be extracted between atrium and apex from theses graphs.

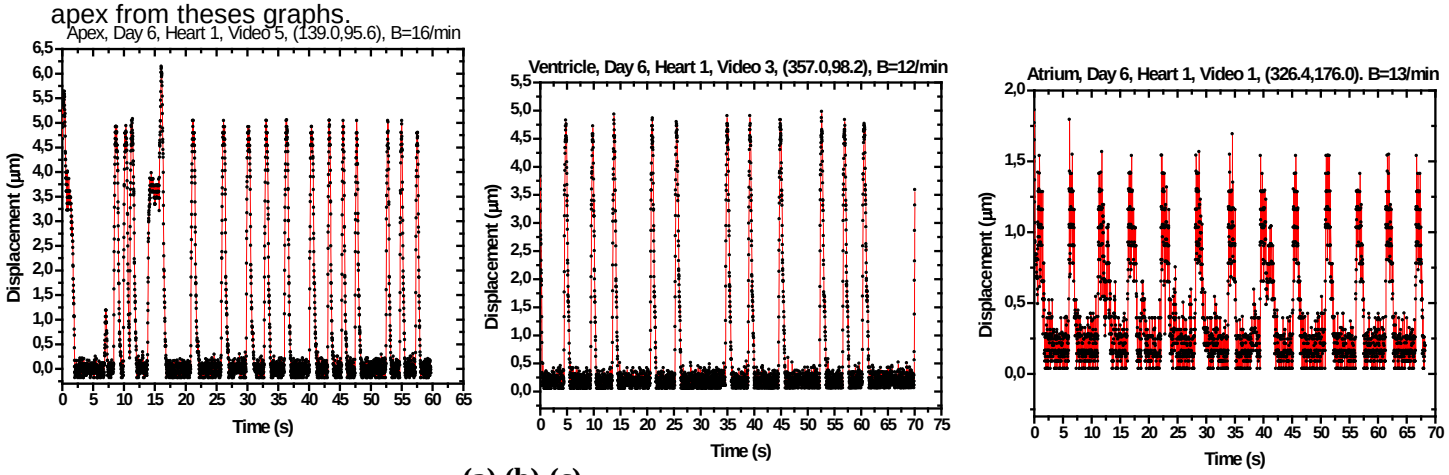

(a) (b) (c)

Figure 4 (a-c)(DMG) of beating myocytes from different segments after 6 days old cell culture. Mechanical connection between myocyte with its neighborhood is visible from each movie. It is remarked that physically the interaction between multiple cells might have electrochemical reason, but optically a displacement tracking is a mechanical observable. Compared to the individual beating of cells, the DMG of interacting myocytes show significant differences. In this situation, the apex and ventricle increased their amplitudes by about 5 times while the atrium gently reduced. Surprisingly, the beating rates don't display any difference between prior and after neighborhood interactivity.

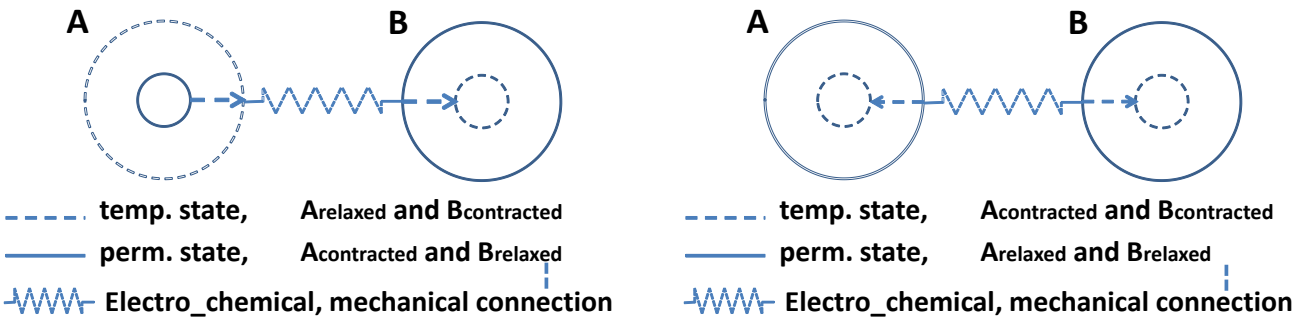

(a) Cell A is relaxing while Cell B is contracting, (b) Cell A and Cell B are contracting simultaneously

Figure 5 Schematical diagram of two dynamical modus: **(a)** both cells are moving in the same direction which means one cell relax while the other contracts. **(b)** both cells contracts at the same time but in opposite directions.

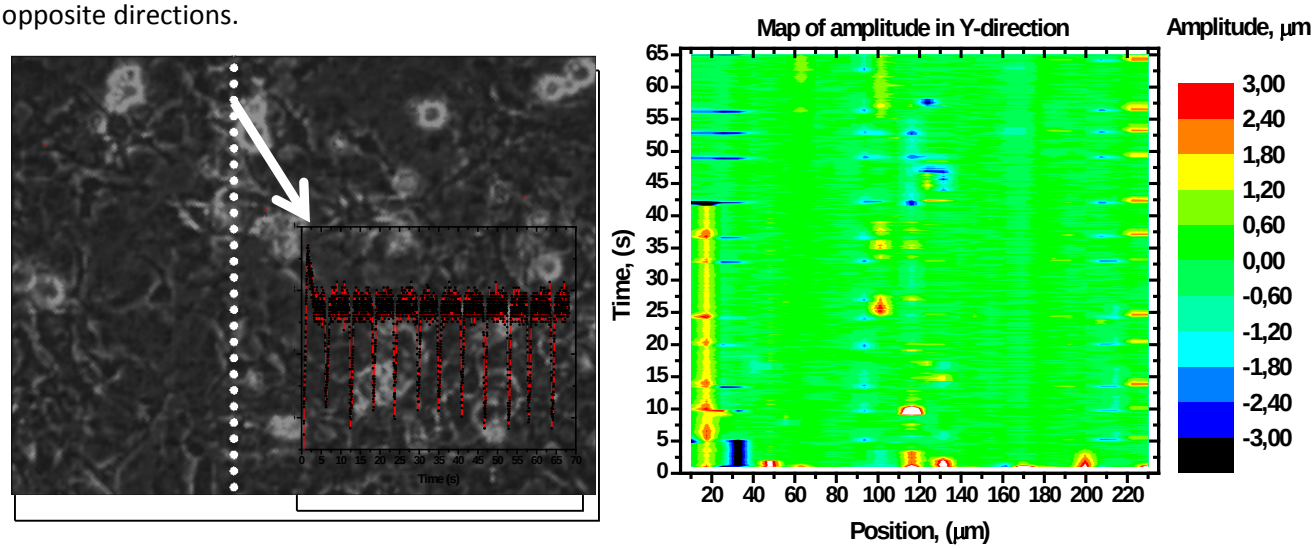

(a) **(b)**

Figure 2 (a) Line visualization of all positions to be tracked. **(b)** Extension from a DMG-curve to a DMG-color-map. Each position in steps of 10µm of the x-axis in image corresponds to a dot along the y-axis in image. The color corresponds to the amplitudes of beating and indicates also the direction of the movement. Thus, the blue color at the position y=210µm has an amplitude of roughly -3.1 µm and means that the membrane moves to the left (negative). At the position y=230 µm the amplitude reaches values of +3.0 µm and moves to the right (positive).

Research Group: Larry Schook

Period Aug'09 to Aug'10

I. **Summary of Work**

We have successfully mobilized stem cells to the peripheral blood in less than 6 hours in the pig model using AMD-3100 (Plerixafor) injections. In conjunction with members of the Kong group, we have also used high elastic modulus, in situ gelling, injectable hydrogels as a vehicle for the delivery of porcine GCSF in the pig stem cell model. This new delivery method enables the slow release of an unstable protein-based therapeutic drug over a period of several days. In addition, we have developed a small animal model of myocardial infarction in order to test materials and methods for myocardial repair prior to deployment in a large animal model.

II. **INTRODUCTION**

The goals of the Schook subgroup are to generate protein and antibody reagents specifically necessary for the mobilization and characterization of porcine stem cells. In addition, we are using animal models of myocardial infarction to test materials and reagents capable of reducing or reversing damaged cardiac tissues.

III. BODY

Stem cell mobilization in the pig (Year 1 milestone #8 and Year 2 milestone #6):

AMD3100 stem cell mobilization: Experiments in stem cell mobilization continued with the use of an alternative mobilization drug, AMD-3100 (also Plerixafor or MOZOBIL). This drug mobilizes stem cells on the order of hours, versus days using the cytokine GCSF (kinetics reported on earlier). Multiple doses of the drug were tested (120, 240, and 480 μg/kg; Figure 1). These experiments determine the kinetics of cell mobilization with the drug.

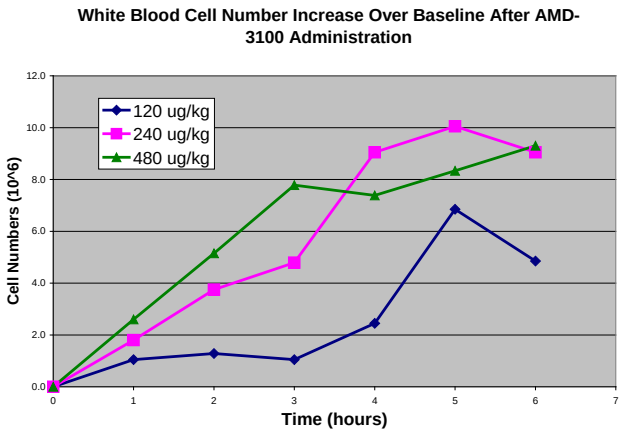

Figure 1. AMD-3100 mediated stem cell mobilization in a pig model. Time zero corrected white blood cell counts are shown over a period of 6 hours post-injection.

In Vivo characterization of controlled release injectable hydrogels: In conjunction with the Kong group, an in situ gelling hydrogel was used to control the release of the stem cell mobilizing drug GCSF in the pig model. This rapidly gelling (<3 minutes) hydrogel degrades quickly in culture over a period of several days. These characteristics prompted its use as a slow release carrier for drug delivery and as a model for injectable hydrogels. The hydrogel was formed via Michael addition reaction between the acrylate groups of poly (ethylene glycol) diacrylate (PEGDA) and primary and secondary amines of poly (ethylenimine) (PEI). Aqueous solutions of PEGDA and PEI were mixed immediately before injection and the hydrogel was formed in under 3 minutes under physiological conditions. The drug is incorporated in the PEI solution prior to mixing. Hydrogel was visualized after injection by incorporating a dye in the mixture. 3mL of the two mixed components, still liquid, were injected into the shoulder of test animals from an unrelated trial immediately after euthanization. Samples were collected approximately 10 minutes after injection. Representative images from four different injections are shown in Fig. 2.

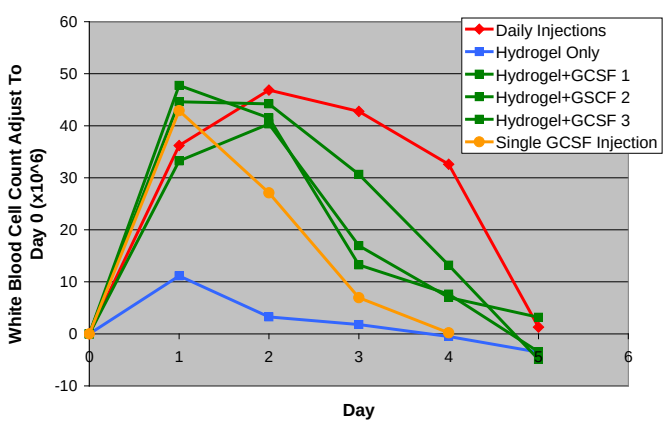

Figure 3. White blood cell counts of pigs injected with GCSF+hydrogel (green lines) are elevated for an extended period of time relative to a bolus injection of GCSF without hydrogel (orange line). White blood cell counts were monitored daily during mobilization. "Daily Injections" consisted of 10μg/kg/day GCSF on day 0 to day 3. "Hydrogel + GCSF" consisted of 40μg/kg injected in 3mL of hydrogel on day 0. "Single GCSF Injection" consisted of 40μg/kg injected without hydrogel on day 0. "Hydrogel Only" consisted of 3mL hydrogel on day 0.

The ability to deliver GCSF from the hydrogels was then tested. Delivery of GCSF + hydrogel increased WBC counts for a sustained period when compared to injection of GCSF alone (Figure 3).

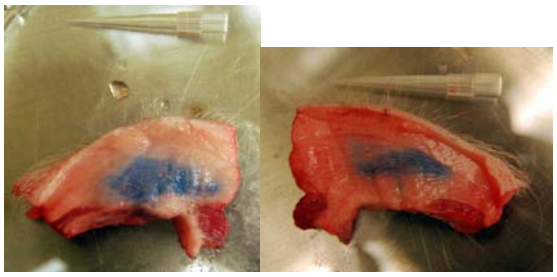

Figure 2. Representative images of in situ gelling hydrogel injected into the shoulder of approximately 40kg pigs. Samples were collected 10 minutes after injection. Hydrogel contained a blue dye for imaging. Pipet tip in images is 5.0cm in length.

Day 4 peripheral blood was cultured in EBM2 media on fibronectin coated cell culture dishes to expand endothelial progenitor cells (EPCs), a potential source of revasculurizing cells. Cultures from GCSF + hydrogel animals developed cells with a typical EPC cobblestone morphology. Both hydrogel only and daily GCSF injection animals developed cells with a fibroblast morphology. Cobblestone cells from

GCSF + hydrogel animals were positive for CD34 and CD31 expression as measured by flow cytometry. Expression of CD34 and CD31 is typical for EPCs. In addition, cobblestone cells were positive for LDL uptake, again typical for EPCs. Fibroblast-like cells were negative for all markers. A manuscript for this work has been submitted to *Biomaterials*.

Mouse myocardial infarction model: We have developed a small animal model as a vehicle for testing different cardiac reagents and materials prior to deployment in large animal models. We received training in a mouse myocardial infarction model from Professor David Geenen at the University of Illinois Chicago. Based on this training we have submitted and received approval for a mouse MI model from the UIUC IACUC. We have also submitted the ACURO paperwork for DoD approval of the model system. As an interim prior to final ACURO approval, we have tested the application of hydrogel patches to mouse hearts using mouse cadavers transferred from other IACUC approved protocols.

A patch consisting of 20% PHEA prepared by members of the Kong group was placed on the surface of a heart in a mouse euthanized approximately 5 minutes earlier using the methods described in the submitted IACUC protocol (Figure 4). The patch adhered lightly by hydrostatic forces. The same patch is shown on the surface of an excised heart. Further testing of materials on live animals will not begin until ACURO paperwork has been approved.

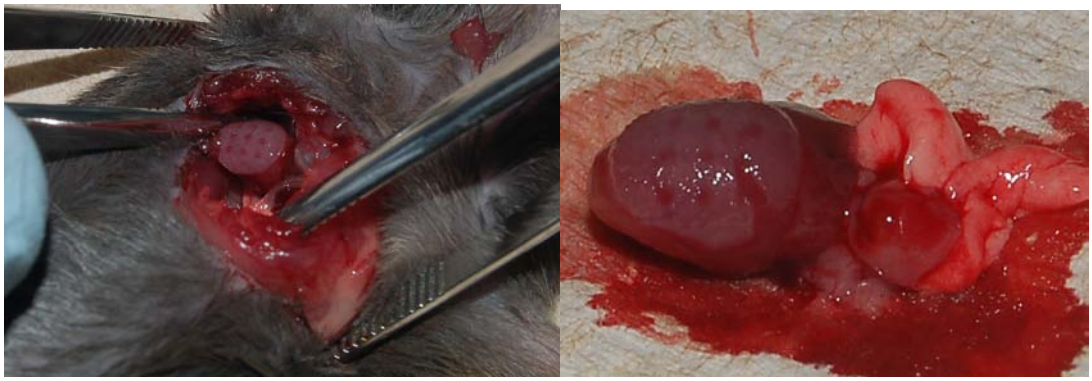

Figure 4. A cardiac "patch" applied to the surface of a mouse cadaver. This model system will be used to test pro-angiogenic, anti-apoptotic materials and reagents following ACURO approval.

IV. KEY RESEARCH ACCOMPLISHMENTS

- AMD-3100 stem cell mobilization and characterization
- Injectable hydrogel for the controlled release of protein drugs
- Mouse model of myocardial infarction

V. REPORTABLE OUTCOMES

- Publication submitted to *Biomaterials*: Liang Y, Jensen TW, Roy EJ, Cha C, DeVolder RJ, Kohman RE, Zhang BZ, Textor KB, Rund LA, Schook LB, ong YW, Kong H. Tuning

the non-equilibrium state of a drug-encapsulated super stiff poly(ethylene glycol) hydrogel for stem and progenitor cell mobilization.

- In Preparation for submission to *Xenotransplantation*: Jensen TW, Swanson DA, Rund LA, and Schook LB. An anti-porcine CD34 antibody recognizes multiple isoforms of porcine CD34.
- American Institute for Chemical Engineering Nov. 8, 2010 National Meeting poster presentation: Liang, Jensen, Roy, DeVolder, Textor, Rund, Schook, Tong, Kong. Independent Control of Elasticity and Drug Release Rate of an Injectable Poly(ethylene glycol) Hydrogel for Stem Cell Mobilization.

VI. CONCLUSION

We have continued to characterize the mobilization of stem cells in the porcine model. The use of AMD3100 enables the rapid (<6 hours) mobilization of stem cells to the peripheral blood. In addition, the use of hydrogel carriers to deliver mobilization proteins can stabilize proteins and prolong their therapeutic impact in vivo. These mobilized cells have been expanded in EPC cultures and have been characterized for the expression of EPC markers in vitro and, for the first time, CD34 expression. We have also developed a small animal model of myocardial infarction that will serve as a bridging technology to test materials and reagents before moving to a more clinically relevant large animal model.

Research Group: Hyunjoon Kong

Period Aug'00 to Aug'10

I. Summary of Work

Kong's group's goal is to develop an advanced cell-encapsulating hydrogel which can support cell viability and function to recreate a cardiac muscle tissue using tissue engineering technology. During the second year, Kong's group focused on developing a novel strategy for constructing a new 'living' microvascular stamp which guides the growth of functional neovessels along its predefined micro-sized pattern in live tissue.

First, Kong's group has prepared a rigid and permeable hydrogel with poly(ethylene glycol) diacrylate (PEGDA) and methacrylic alginate (MA), so that the cell-encapsulated hydrogel would not only remain stable at the implanted site but also support cellular expression of proangiogenic factors.

Second, Kong's group created the microvascular stamp by incorporating microchannels with controlled diameter and spacing into a fibroblast-encapsulated hydrogel using a 3-D stereolithographic fabrication technique. Using this stamp, we have demonstrated that we can orchestrate the hydrogel proangiogenic factors along the circular cross-section of the microchannel and form the neovascular pattern equivalent to the pattern engraved into the stamp.

The result of our study will be an invaluable paradigm of a 3D cell encapsulation device prepared with a broad array of gel-forming polymers. Specifically, the stamp created in this study will become a powerful tool to better understand vascular biology and also improve quality of a variety of clinical treatments necessitating the neovascularization.

II. INTRODUCTION:

Kong's group's goal is to develop a novel cell encapsulating hydrogel which can be readily integrated with a stereolithographic apparatus (SLA) and also presents chemical and mechanical properties proper to support cellular viability, growth, differentiation, growth factor secretion and eventually engineer the spatial organization of neovessels. Specifically, we had focused on achieving two sub-goals; 1) Develop methods to decouple the dependency of hydrogel mechanics on the swelling ratio, so we could control the gel stiffness without significantly altering hydrogel permeability, and 2) Develop a cell-encapsulating vascularized bioactive hydrogel, so we could enhance the cellular viability and diverse activities including growth, differentiation and growth factor secretion, eventually engineer the spatial organization of neovessels in live tissues.

III. BODY:

A. A rigid and permeable hydrogel matrix.

Hydrogels are increasingly being used as cell encapsulation devices for both fundamental biology studies and cell transplantation thereapies because of their structural similarity to the natural extracellular matrix. The successful use of a hydrogel greatly relies on an ability to control hydrogel stiffness which affects structural integrity and regulates cellular phenotypes. However, conventional strategies to increase the gel stiffness lead to decrease in the gel permeability and subsequently deteriorate the viability of cells encapsulated in a gel matrix. Therefore, in this study, the elastic modulus and swelling ratio of the poly(ethylene glycol) diacrylate (PEGDA) hydrogel were tuned to prepare a rigid and permeable hydrogel, so that the cell-encapsulated hydrogel would not only remain stable at the implanted site but also support cellular expression of proangiogenic factors. Increasing the total polymer concentration of the PEGDA hydrogel showed an increase in elastic modulus and a decrease in swelling ratio, which is the typical inverse relationship between stiffness and bulk permeability of conventional hydrogel systems (Figure 1(b)). In contrast, the hydrogel consisting of PEGDA and synthetic methacrylic alginate (MA) (Figure 1(a)) which presents multivalent methacrylic groups and hydrophilic hydroxyl groups showed an increase in both elastic modulus and swelling ratio with the mass fraction of MA (Figure 1(c)).

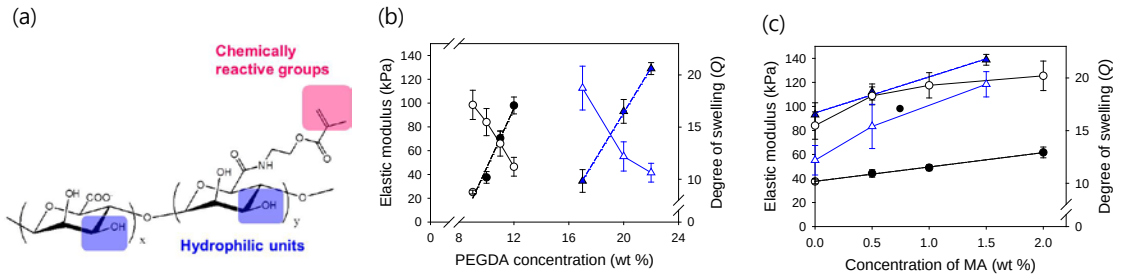

Figure 1 Schematic diagram of the methacrylic alginate (MA) (a). Increasing polymer concentration of the pure PEGDA hydrogel resulted in the increase of elastic modulus (● for PEGDA700 and ▲for PEGDA1000) and the decrease of degree of swelling (○ for PEGDA700 and Δ for PEGDA1000) (b). In contrast, increasing mass fraction of MA in the PEGDA-MA hydrogel while keeping total polymer concentration led to increases of both the elastic modulus (● for PEGDA700-MA and ▲for PEGDA1000-MA) and the degree of swelling (○ for PEGDA700-MA and Δ for PEGDA1000-MA) (c).

B. Microvascular stamp for neovascularization.

Neovessels play a critical role in homeostasis, regeneration, and pathogenesis of tissues and organs, and their spatial organization is a major factor to influence the vascular function. It has been proposed that an ability to control growth direction and spacing of neovessels over physiologically relevant length scales can provide a better understanding and controllability of neovessel formation. However, a technology to accomplish this challenging goal is still lacking. Here, we present a microvascular stamp which releases multiple proangiogenic factors along its predefined micro-sized pattern to engineer the spatial organization of neovessels.

B.1. Control of microchannels' size and spacing

Microchannels with controlled spacing were introduced into the PEGDA-MA hydrogels with the goal of driving neovessel growth along its circular pattern. We hypothesize that neovessel growth direction can be controlled by increasing the flux of the cell-secreted proangiogenic factors through the microchannel wall, so that the neovessels localize within the microchannel lumen (Figure 2(a)). According to Fick's law of diffusion, the ratio between the flux of growth factors through the microchannel wall of the stamp (J_m) and the flux through the bottom of the stamp with the same cross-sectional area as the microchannel (J_f) is equal to the ratio between the surface area of microchannel wall (S_{wall}) and the cross-sectional area of the microchannel (S_{bottom}). Hence, for a hydrogel with thickness of 200 μm, it could be predicted that the diameter of the microchannels should be less than 800 μm in order to make J_m larger than J_f. Based on this prediction, microchannels with diameter (d) of 500 μm were fabricated in the PEGDA and PEGDA-MA hydrogels using the stereolithographic apparatus (SLA) (Figure 2(c)).

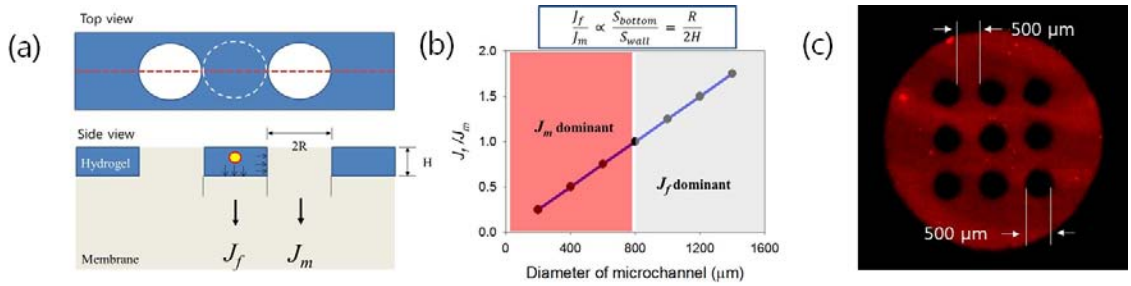

Figure 2 (a) It was hypothesized that the flux of cell-secreted growth factors released through a microchannel wall of a hydrogel (J_m) should be larger than that released through the bottom of a gel with the same cross-sectional area as the microchannel (J_f) in order to control the growth pattern of neovessels. (b) A modeling based on the Fick's law of diffusion suggested that J_m should be larger than J_f as the microchannel diameter becomes smaller than 800 μm with a hydrogel with thickness of 200 μm. (c) Following the model-based calculation, microchannels with diameter of 500 μm were incorporated into the hydrogel via the bottoms-up process with SLA.

B.2. Characterization of permeability of the PEGDA and PEGDA-MA hydrogels

The hydrogel permeability was evaluated by monitoring water diffusion into the hydrogel with magnetic resonance imaging (MRI) (Figure 3). Despite the higher stiffness of the PEGDA-MA hydrogel compared to the PEGDA hydrogel, water diffused into the PEGDA-MA hydrogel more rapidly. Further, the diffusivity (D) of water into the PEGDA-MA hydrogel as calculated from MRI image was significantly increased due to the presence of microchannels. This was also confirmed by calculating the diffusivity which was found to be 3.14×10^{-8} cm^2/s for PEGDA-MA with microchannels, 2.6×10^{-8} cm^2/s for PEGDA-MA and 1.2×10^{-8} cm^2/s for PEGDA hydrogel. The MRI images showed that water diffused into the hydrogel more exclusively through microchannel walls and ultimately led to a faster increase in the amount of water bound to the gel matrix than the microchannel-free hydrogels.

B.3. Patterning of functional neovessels using the microvascular stamp

Fibroblast-encapsulated hydrogels were implanted onto chorioallantoic membrane (CAM) to validate whether the bulk permeability and microchannel geometry of the hydrogels affected the creation of neovessels formation. Implantation of the microchannel-free PEGDA hydrogel onto the CAM (Figure 4(a)) stimulated inflammation within two days, most likely because of extravasation of the debris from the dead cells (Figure 4b-1). This result was similar to inflammation stimulated by a fractured hydrogel that physically exposed the encapsulated cells

to host tissue. In contrast, the microchannel-free PEGDA-MA hydrogel minimally stimulated host inflammation, most likely because of its ability to increase the viability of encapsulated cells. However, no specific pattern of neovessels was found with the microchannel-free hydrogels (Figure 4b-1 & 4b-2). Remarkably, implantation of the PEGDA-MA hydrogel containing microchannels with diameter of 500 μm stimulated the growth of neovessels along its circular pattern. The spacing between the circular neovessels was the same as that between the microchannels introduced into hydrogel (Figure 4b-3). Such patterning of neovessels was not achieved with the same hydrogel loaded only with VEGF, rather than the fibroblasts.

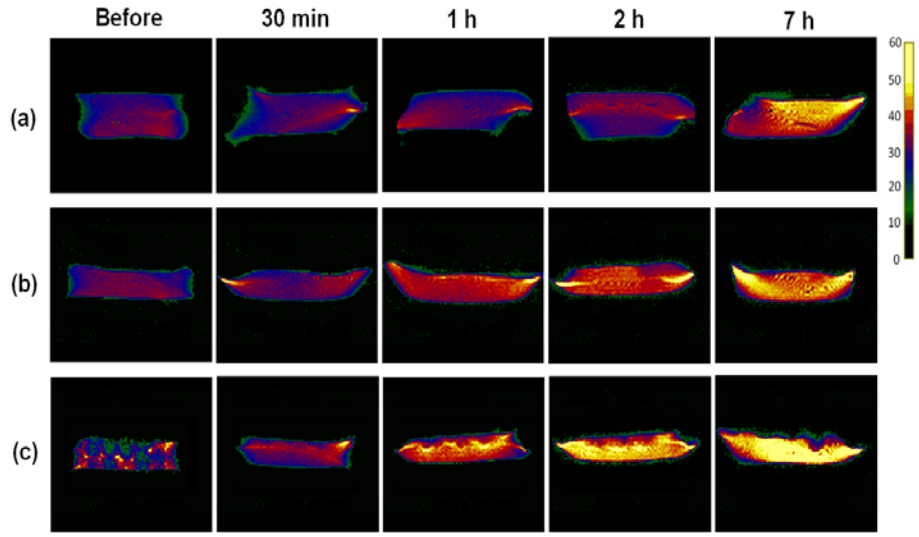

Figure 3 Water protons visualized with MRI were diffused into PEGDA-MA hydrogel (b) more rapidly than the pure PEGDA hydrogel (a). Further, water protons imaged with MRI diffused into the PEGDA-MA hydrogel more preferably through the microchannel wall (c), leading to the faster water diffusion than the microchannel-free hydrogel. Pseudo-color of MRI images represents the intensity of water proton (see the scale bar on the right).

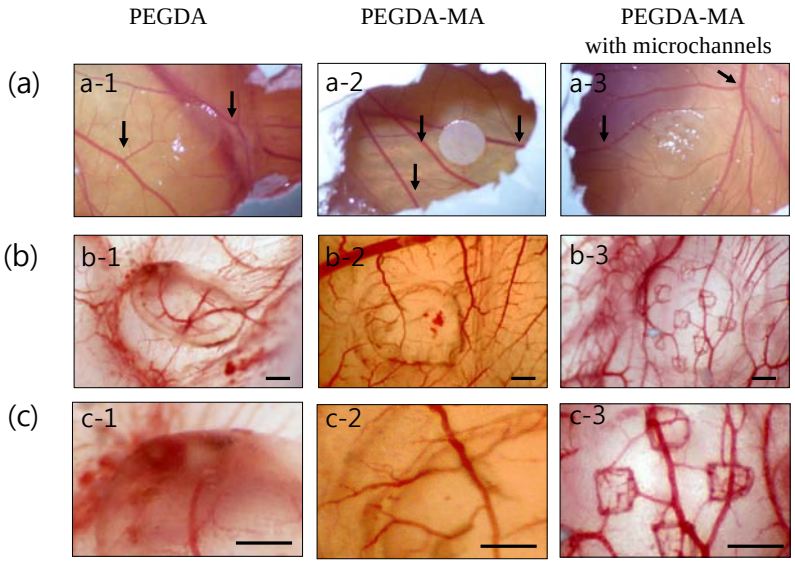

Figure 4 (a) Images shown were captured right after the cell-hydrogel constructs were implanted. Arrows in (a) represent blood vessels existed before implantation of the cell-hydrogel construct. (b) Images displayed represent top views of the CAM exposed to the cell-hydrogel construct for seven days. The implantation of PEGDA-MA hydrogel with microchannels (diameter = 500 μm) uniquely resulted in neovessels grown along the circular pattern of microchannel in the hydrogel (b-3). In addition, the spacing between the

IV. KEY RESEARCH ACCOMPLISHMENTS:

- Synthesize bioactive, bio-degradable methacrylic alginate (MA) and demonstrate hydrogel fabrication with stereo-lithographic apparatus.

  - Kong's group has synthesized the methacrylic alginate (MA) and further combined the MA and PEG diacrylates to control the hydrogel stiffness and swelling ratio in an independent manner.
  - The hydrogel incorporated with MA was used as an effective cell-encapsulation device which enhanced the cell viability and proangiogenic growth factors secretion from cells.
  - The methacrylic alginate-PEGDA hydrogel was combined with the SLA unit to assemble the vascularized 3D tissue engineering scaffold, which is expected to improve the cell viability and activities in a 3D matrix.

- Develop a method to characterize the permeability of hydrogel by the Magnetic Resonance Imaging (MRI)

  - Kong's group has recently developed a method to characterize the permeability of hydrogel by monitoring the diffusion of water protons into the hydrogel using magnetic resonance imaging (MRI) and calculated the diffusivity in different geometries.

- Design of 'living' microvascular stamp for neovascularization.

  - Kong's group has developed a novel strategy for constructing a new 'living' microvascular stamp which guides the growth of functional neovessels along its predefined micro-sized pattern in live tissue.
  - Using the stamp, Kong's group has demonstrated that we could orchestrate the hydrogel properties and the microchannel geometry to release the cell-secreted proangiogenic factors and form the neovascular pattern equivalent to the pattern engraved into the stamp.

V. REPORTABLE OUTCOMES:

- List of papers published in peer-reviewed Journals
  - Cha, C., Kohman, R. and Kong, H.J., Biodegradable polymer crosslinker: Independent control of stiffness, toughness, and nydrogel degradation rate. *Advanced Functional Materials* (2009) 19, 1-7
  - C. Cha, S. Kim, L. Cao, H.J. Kong, "Decoupled control of stiffness and permeability of cell-encapsulated poly(ethylene glycol) hydrogel," *Biomaterials* 31, 4864-4871 (2010).

- List of abstracts and presentations in related conferences

- J.H. Jeong, V. Chan, C. Cha, Z. Pinar, R. Bashir, and H.J. Kong, “In situ Cell Encapsulation into a vascularized hydrogel matrix using a SLA.” Advances in Tissue Regenerative Symposium at UIC, Chicago (March 2010). “Awarded honorable mention.”
- J.H. Jeong, V. Chan, C. Cha, Z. Pinar, R. Bashir, and H.J. Kong, “Assembly of Vascularized Cell-Encapsulated Hydrogel Matrix using a Stereolithography.” 2010 International Conference on Biofabrication, Philadelphia (October 2010)
- J.H. Jeong, V. Chan, C. Cha, Z. Pinar, R. Bashir, and H.J. Kong, “Design of Vascularized Cell-Encapsulated Hydrogel Matrix for neovascularization.” Accepted to 2010 Materials Research Society (MRS) Fall Meeting, Boston (November 2010)

CONCLUSION:

Kong’s group hypothesized that a construct capable of releasing multiple proangiogenic growth factors along a pattern engraved into that construct, while maintaining its structural integrity at the implant site, would generate the desired vascular pattern. We examined this hypothesis by encapsulating cells that were reported to endogenously express multiple proangiogenic growth factors into a rigid but permeable hydrogel of poly(ethylene glycol) (PEGDA) and methacrylic alginate (MA). In this manner, the cells were stimulated to release the soluble factors in a sustained and responsive manner. Furthermore, using a stereolithography fabrication unit, microchannels of appropriate diameter and spacing guided by Fick’s law of diffusion, were incorporated into the cell-encapsulating hydrogel, so the flux of growth factors through the walls of the microchannels would be much larger than that through other parts of the hydrogel. The hydrogel permeability was evaluated by monitoring water diffusion into the hydrogel with magnetic resonance imaging (MRI), and the function of the microvascular stamp to control neovessel formation was examined by implanting it onto a chick embryo membrane (CAM).

Using this stamp, Kong’s group have demonstrated that we can orchestrate the hydrogel properties and the microchannel geometry to release the cell-secreted proangiogenic factors along the circular cross-section of the microchannel and form the neovascular pattern equivalent to the pattern engraved into the stamp. Controlling the ‘bottoms-up’ emerging behavior of the neovessel formation via ‘directed top-down’ cues using the living microvascular stamp can be a major step forward in tissue engineering. We therefore propose that the resulting microvascular stamp will become a powerful tool to better understand vascular biology and also improve quality of a variety of clinical treatments necessitating the neovascularization.

VI. REFERENCES:

(1) Lee K.Y., and Mooney D.J., *Chem. Rev.* 2001, 101, 1869

(2) Lou X., Chirila T.V., *J. Biomater. Appl.* 1999, 14, 184

(3) Kong H.J., Wong E., and Mooney D.J., *Macromolecules* 2003, 36, 4582

(4) Kong H.J., Smith M.K., and Mooney D.J., *Biomaterials* 2003, 24, 4023

(5) Fischbach, C., Kong H.J., Hsiong S., Evangelista M., Yuen W., and Mooney D.J., *PNAS (USA)* 2009, 106, 399

(6) De S., Razorenova O., McCabe N.P., O'Toole T. Qin J. and Byzova T.V., *PNAS (USA)* 2005, 102, 7589

(7) Karina A., Brenda K., and Wicker R.B., *Annals of Biomedical Eng.* 2006, 34, 1429

(8) Dorfleutner, A., Carmeliet, P., Mueller, B.M., Friedlander, M. & Ruf, W. *Nature Medicine* 2004, 10, 502-509

(9) Chen, R.R., Silva, E.A., Yuen, W.W. & Mooney, D.J. *Pharm. Res.* 2007, 24, 258-264

VII. APPENDICES:

VIII. Any other information relevant to the project

Research Group: Brian Cunningham

Progress Report on label free imaging of cell adhesion using photonic crystals

We have established significant progress toward resolving changes in cell attachment using photonic crystal biosensors. After optimizing our instrumentation and device design, we have improved our image quality and the reliability of our biosensor configuration. Using this updated configuration, we have successfully monitored the growth and proliferation of several cell types, including Panc-1 pancreatic cancer cells, mouse cardiomyocytes, and HepG2 hepatic carcinoma cells, among others. Furthermore, we have demonstrated the ability to resolve cellular responses to a range of stimuli including pro-apoptotic drugs and a number of ECM coatings. With continued work, we plan to increase the complexity and length of our studies with regard to cell attachment and proliferation using photonic crystal biosensors.

Instrumentation

We have made several changes to the microscope and device configuration to improve both the optical resolution and device sensitivity. We implemented a diode laser to reduce the appearance of interference fringes appearing due to partial reflection of the laser light as it is transmitted through the sample. The increased coherence length of the original 633nm HeNe source caused wide fluctuations of the intensity at angles above resonance. Figure 1 shows intensity as a function of angle curves for the 633nm HeNe laser (left) and the newly implemented diode laser (right).

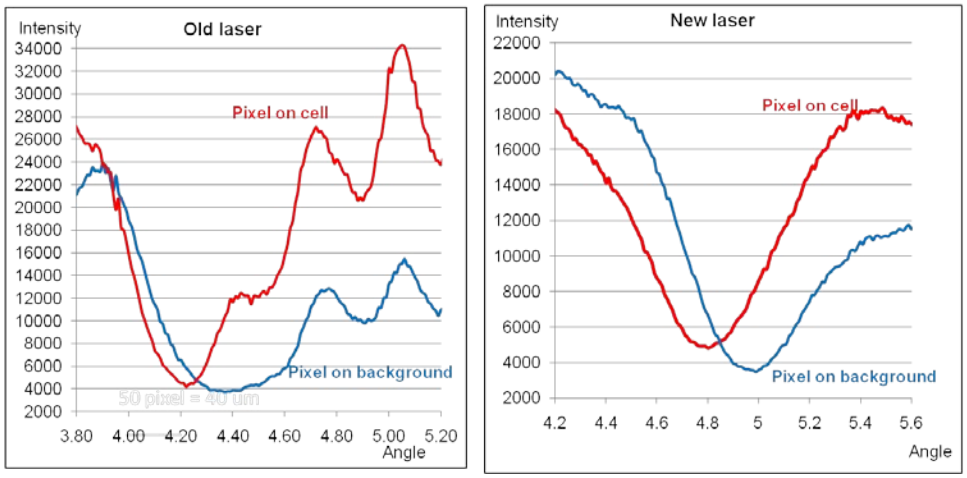

Figure 1: The new diode laser generates smoother curves, allowing less problematic determination of the shifts in angle of minimum transmission caused by cell attachment.

We have also altered the device configuration to allow for higher sensitivity. The devices are now made with a 25 nm grating depth, 360 nm period followed by a 200 nm layer of SiO2. Then TiO2 is

sputtered onto the SiO2 until the device resonance is approximately 30 nm below the laser wavelength. This configuration leads to a resonance angle between 3 and 5 degrees and peak width of 4-5 nm.

In order to promote cell attachment to the sensor surface, coating protocols have been developed whereby the TiO2 layer is covered with organic molecules amenable for cell culture. Either poly-d-lysine or fibronectin followed by collagen are used, both of which have proven to work with the biosensor. With this optimization, we have been able to detect cell attachment after only one hour of seeding the cells on the sensor surface.

The imaging principle is depicted in Figure 2. The left image was taken at an angle 1° below background resonance and is therefore similar to a regular bright field image. The image to the right was taken at an angle where the background is at resonance and appears dark due to the light coupling into the grating structure. At locations where a cell is attached the resonance angle is shifted and those areas therefore display a higher light intensity. The graph in the figure shows the intensity-versus-angle curves for a pixel on the cell and a pixel on the background demonstrating the underlying imaging principle of this technique. The figure on the right shows the corresponding AMT image displaying the angle shift per pixel with respect to the background average. The color bar denotes the values of the shift with 0 representing the background average. Since the AMT image is created from bright field images, the latter ones can be used to validate this new imaging technique. By overlaying the AMT with a bright field image the area of the cell interacting with the substrate can be compared with the visible area and shape of the cell.

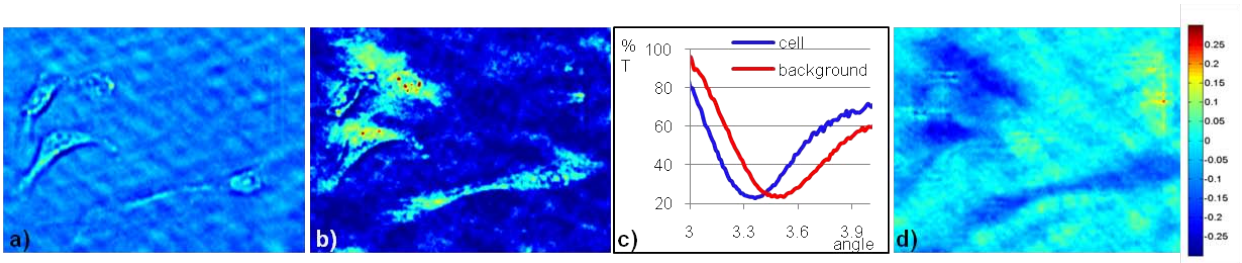

Figure 2: Bright field images help to establish regions of interest (a-b), while the Angle of Minimum Transmission images display attachment data for the entire field (c-d).

Apoptosis Induction in Panc-1 Pancreatic Cancer Cells

Panc-1 cells have been used first to test the capabilities of the instrument since they are easy to culture on the device and adhere readily. Figure 3 shows the process of attachment of panc-1 cells over the course of 4 hours.

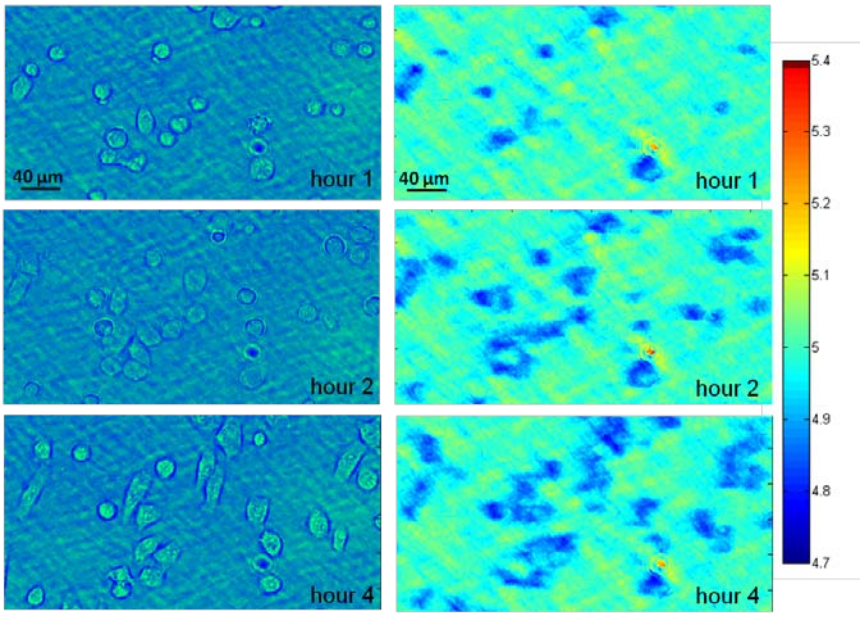

Figure 3: Panc-1 cells show increased AMT shift over a period of hours after being introduced to the biosensors and cultured at 37°C.

The left column shows bright field images and the right column the corresponding label free images displaying the angle of minimum transmission (AMT). The color bar denotes the values of the AMT. Whereas the bright field images show all cells that have settled onto the surface, the AMT images only display those that are interacting with the substrate, i.e. have attached to the surface. When comparing the two image types, it can be seen that some cells are already attached after one hour whereas others have only settled down. After two hours the area of attachment has greatly increased. After four hours the cells have become more elongated and this change in cell shape is well reflected in the AMT images. Statistical analysis of the AMT images revealed that the cells cause a shift in AMT of 0.17 degrees with respect to the background average. The standard deviations over the pixels on a single cell were between 9 and 16% of the average shift of that cell.

In a different experiment panc-1 cells were incubated on the device for 24 hours and then treated with staurosporine, an apoptosis-inducing agent at 5 µg/ml. The response was analyzed by examining individual pixels on the cell (Figure 4).

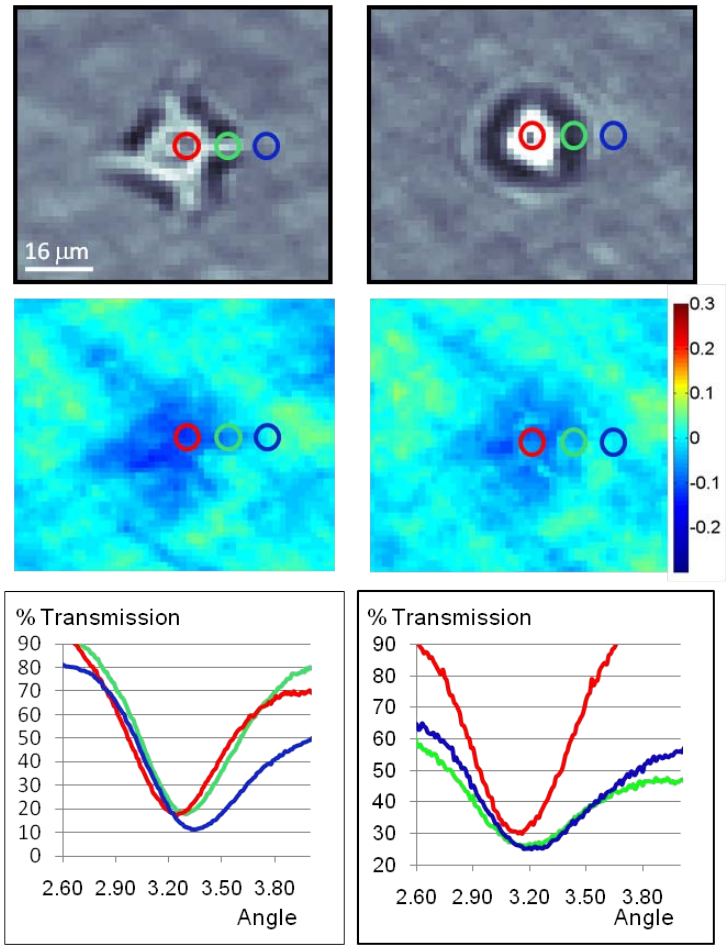

Figure 4: Treatment of Panc-1 cells with staurosporine results in decreased AMT shift and pronounced changes in cell morphology, most notably along cell projections to the surrounding extracellular matrix.

At the top of the figure the bright field images before and one hour after treatment demonstrate how the cell has rounded up in response to the toxin. The corresponding AMT images below show a similar change in shape. The pixel analyses for the marked regions (red: cell center, green: right arm of cell, blue: background) before and after treatment are given in the graphs below. Before treatment the cell center and its arm give the same shift of approximately 0.1° with respect to the background. One hour after treatment the cell arm has been retracted and the shift represented by the green curve has moved back to background values. Since the cell remains on the surface its center still causes a slight shift albeit smaller than before treatment indicating a weakening of attachment. This is evidence that once a cell or a part of a cell detaches from the sensor surface the original sensor conditions are restored.

Growth and Proliferation of HepG2/C3 Hepatic Carcinoma Cells

As comparison to panc-1 cells human liver cancer cells of the line HepG2/C3 were plated on a sensor surface and process of their attachment was imaged after 1, 2, 4 and 23 hours (Figure 5). The following figure shows the bright field images at the top and the corresponding label free AMT images at the bottom. Contrary to the panc-1 one hour after seeding all cells are clearly visible on the AMT image and they shift the local resonance angle by 0.25 degrees on average with a standard deviations across four cells of 4% of the shift. The three cells forming a cluster are not resolved in the AMT image indicating that their areas of attachment overlap. With increasing time the cells change their shape and become more elongated. The cell at the top of the images changes its position and moves downward and to the right. The figure clearly demonstrates how the AMT images follow the observed changes in the bright field images lending strong proof to the concept of this imaging technique.

The dark blue color in the cell centers seen in the AMT images, indicates that the attachment is the strongest here. With increasing time the area of cell attachment expands and the cells grow longer extensions at their perimeters. This spread out attachment makes the AMT image after 23 hours image look diffuse. It becomes clear that the area of the cell interacting with the substrate is substantially larger than the bright field images indicate.

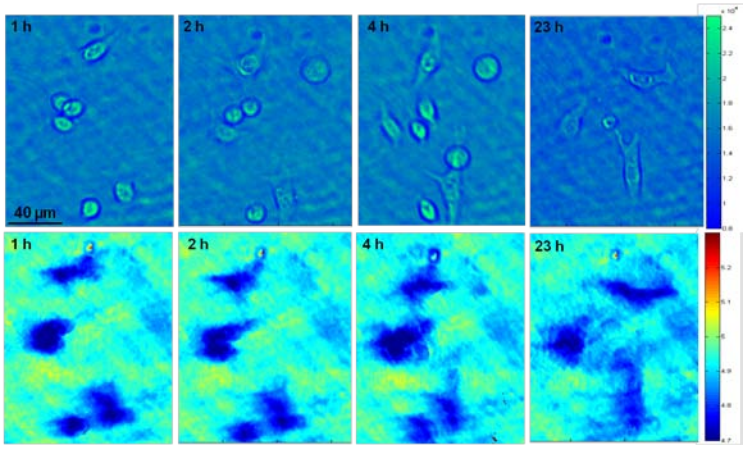

Figure 5: HepG2/C3 hepatic carcinoma cells establish strong attachment after less than an hour; evidence of movement and changes in intercellular associations is shown up to 23h in culture.

Cardiomyocytes

After successfully demonstrating the ability to study cell attachment with this microscope we used the instrument to examine the influence of strength of attachment on the beating of cardiomyocytes. Cardiomyocytes were isolated from rat heart and directly plated onto the sensor coated with fibronectin and collagen. Images were taken after one and two days (Figure 6). The cells started beating on the second day. Analysis of the AMT images revealed that those cells that displayed

significant shifts- meaning that they were well adhered to the surface- were more likely to beat than those weakly attached.

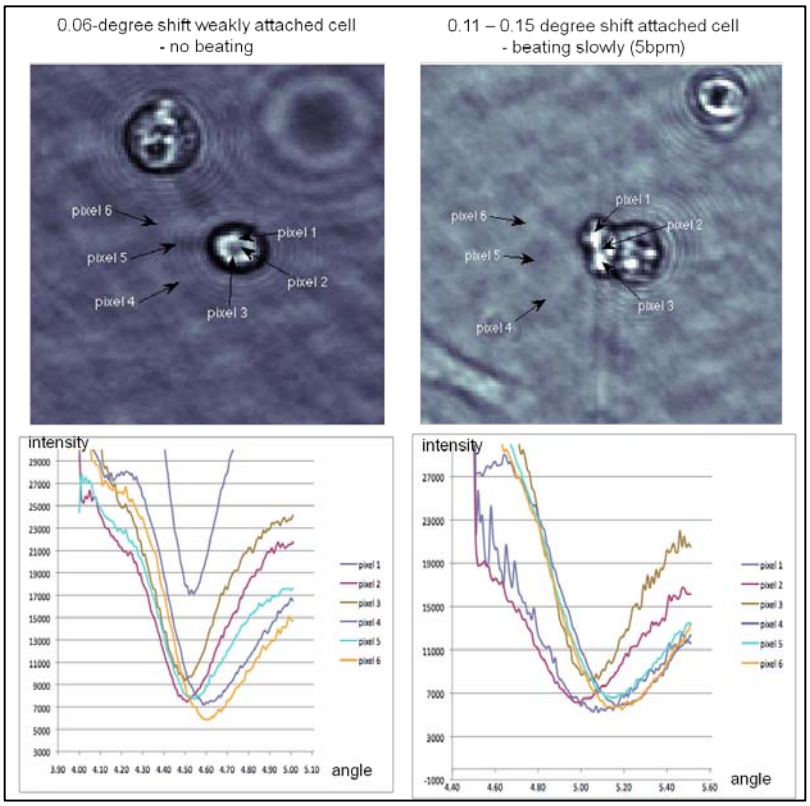

Figure 6: The upper row shows the bright field images and the lower row the intensity-versus-angle curves for the pixels marked on the images.

Summary

We have demonstrated label-free imaging of cell attachment for a variety of cell types including panc-1, HepG2/C3 and cardiomyocytes. The instrument has the ability to monitor changes in cell adhesion over a 24-hour period at the level of individual cells, and to monitor the distinct behavior of individual cells within a population. Furthermore, we have established that he biosensor can detect differences in the strength of attachment within individual cells and across different cells and to measure changes induced by exposure to drugs. We are continuing to pursue similar studies to optimize cardiomyocyte cell culture by changing ECM components. Through the use of label-free microscopy using photonic crystal biosensors, we will gain helpful information for defining more effective cardiomyocyte culture protocols in the future.